



CHALMERS
UNIVERSITY OF TECHNOLOGY

Mechanistic Insights into the Induction Period of Methanol-to-Olefin Conversion over ZSM-5 Catalysts: A Combined Temperature-Programmed

Downloaded from: <https://research.chalmers.se>, 2026-04-05 10:58 UTC

Citation for the original published paper (version of record):

Omojola, O. (2023). Mechanistic Insights into the Induction Period of Methanol-to-Olefin Conversion over ZSM-5 Catalysts: A Combined Temperature-Programmed Surface Reaction and Microkinetic Modeling Study. *Industrial & Engineering Chemistry Research*, 62(36): 14244-14265.
<http://dx.doi.org/10.1021/acs.iecr.3c01401>

N.B. When citing this work, cite the original published paper.

Mechanistic Insights into the Induction Period of Methanol-to-Olefin Conversion over ZSM-5 Catalysts: A Combined Temperature-Programmed Surface Reaction and Microkinetic Modeling Study

Toyin Omojola*



Cite This: *Ind. Eng. Chem. Res.* 2023, 62, 14244–14265



Read Online

ACCESS |



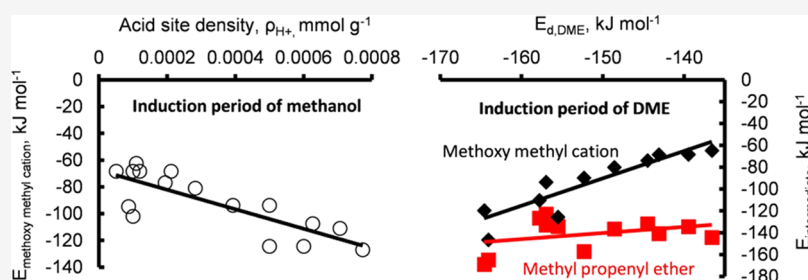
Metrics & More



Article Recommendations



Supporting Information



ABSTRACT: The induction period of propylene formation from methanol is compared to that of dimethyl ether (DME) over ZSM-5 catalysts of different compositions using a combination of temperature-programmed surface reaction experiments and microkinetic modeling. Transient reactor performance is simulated by solving coupled 1D nonlinear partial differential equations accounting for elementary steps based on the methoxy methyl mechanism and axial dispersion and convection in the reactor. Three binding site ensembles and three active site ensembles are observed. These sites constitute up to 3% (binding sites ~70%, active sites ~30%) of the total acid sites during methanol conversion and up to 1% (binding sites ~30%, active sites ~70%) of the total acid sites during DME conversion. Over the binding sites, during the induction period of methanol, and DME conversion, the acid site density is the key descriptor. Over the active sites, acid site density is the key descriptor with higher site densities correlating with lower barriers of propylene formation during the induction period of methanol conversion. The barrier to DME desorption is the key descriptor, with lower desorption barriers correlating with lower barriers of propylene formation during the induction period of DME conversion. Barriers to propylene formation are lower during the induction period of methanol conversion (up to 141 kJ mol^{-1}) compared to that of DME conversion (up to 200 kJ mol^{-1}) over ZSM-5 catalysts.

INTRODUCTION

The conversion of methanol to hydrocarbons (MTHs) over zeolite catalysts was first reported in 1977,¹ and in the late 1990s, methanol-to-olefin (MTO) conversion was used for on-purpose generation of propylene (MTP) using natural gas, coal, or biomass as feedstock. These alternative feedstocks are first converted to synthesis gas, which is later liquefied to methanol and subsequently transformed into propylene.² As the demand for propylene is expected to increase faster than its production, on-purpose propylene processes such as MTP are required to close the propylene gap.³ At low pressures and high temperatures, the product distribution during methanol conversion over ZSM-5 catalysts can be tuned toward light olefins^{4,5} due to its cracking chemistry.

Before steady state is reached, the early stages of the conversion of methanol to olefins consist of an induction period and a transition regime.⁶ During the induction period, starting molecules diffuse and adsorb into the pores of the ZSM-5 catalyst. Thereafter, the first carbon–carbon (C–C) bond and primary olefins form, which subsequently desorb and diffuse out

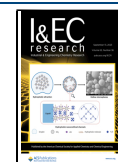
of the ZSM-5 pores. During the transition regime, the onset of the propagation of the dual cycle⁷ begins. The primary olefins, i.e., ethylene and propylene, which are formed during the induction period, initiate the olefin cycle by surface methylation with methanol and/or dimethyl ether onto higher homologues ($\text{C}_6^=$). These higher olefin homologues undergo hydrogen transfer and cyclization to lower aromatics, which initiate the aromatic cycle by surface methylation with methanol and dimethyl ether onto higher aromatics. These higher aromatics subsequently dealkylate to lower aromatics and olefins. Ethylene and aromatics are mechanistically separated from propylene and higher olefins.⁷ The dual cycle, consisting of the olefin and aromatic cycle, is fully functional at steady state over ZSM-5

Received: April 27, 2023

Revised: July 27, 2023

Accepted: July 28, 2023

Published: August 28, 2023



catalysts.⁸ In effect, the early stages of MTO conversion can be grouped into the induction period where the first C–C bond and primary olefins are formed; the transition regime, where the primary olefins initiate the dual cycle; and the steady state, where the dual cycle is fully functional. During this chemical process, the active sites are transformed through proton mobility⁹ and clustering^{10,11} of adsorbed molecules.

The formation of the first C–C bond and primary olefin(s) from methanol during the induction period has been debated for over 45 years. This has led to about 20 distinct mechanisms, with increasing evidence for the direct mechanisms. The direct mechanisms for the formation of the first C–C bond include the carbene mechanism,^{12–14} multiple analogues of the oxonium,¹⁵ methane-formaldehyde mechanisms,^{16,17} methyleneoxy mechanism,¹⁸ surface methoxy groups,^{14,19–21} methoxy methyl mechanism,^{22,23} and the carbon dioxide mechanism, which leads to the formation of methyl acetate and acetic acid.^{24–28} The methoxy methyl mechanism allows for the formation of dimethoxyethane as the first C–C bond during propylene formation.^{22,23}

As the first C–C bond is formed, active sites are transformed during the induction period. Active sites are transformed into organic reaction centers,²⁹ supramolecular active centers,³⁰ and hydronium ions (in the presence of water)³¹ as steady state is reached. Clustering of adsorbed molecules^{10,11,32,33} and proton mobility^{9,34} occurs. The transformation of active sites and the formation of the first C–C bond during the induction period of methanol conversion can be studied using a combination of temperature-programmed surface reaction (TPSR) and microkinetic modeling studies. Here, the catalyst is subjected to a temperature ramp during the induction period, and fitting a mechanistic model allows the extraction of kinetic parameters and scaling relationships that are relevant to catalyst design. These relationships are necessary to develop a framework where several parameters governing the structure, morphology, composition (Si/Al ratio), and the presence of various ions can be used to fine-tune the number, nature, strength, and distribution of acid sites.^{35–38}

This integrated temperature-programmed surface reaction approach complements our previous studies through a reductionist approach that aim to decouple the adsorption, desorption, activity, and diffusion through an individual combination of temperature-programmed desorption,³² competitive adsorption,³⁹ temperature-programmed surface reaction,^{40,41} step response,^{6,42} and quasi-elastic neutron scattering^{43,44} studies to probe the formation of primary olefins from methanol over fresh and working ZSM-5 catalysts. The novelty in this work is that we present new data on the temperature-programmed surface reaction of methanol over fresh and working ZSM-5 catalysts of Si/Al ratios of 25, 36, and 135 and additional experimental data on the temperature-programmed surface reaction of dimethyl ether over fresh and working ZSM-5 catalysts of a Si/Al ratio of 25. In both cases, we present and use a microkinetic model based on the methoxy methyl pathway to extract descriptors for the formation of propylene during the induction period of methanol and dimethyl ether conversion over ZSM-5 catalysts of varying compositions.

We observe that the acid site density and activation energy of DME desorption are key descriptors during the induction period of propylene formation. The acid site density is the key descriptor over the binding and active sites of ZSM-5 catalysts during the induction period of methanol conversion. Higher site densities correlate with lower barriers to propylene formation.

While the acid site density is the key descriptor over the binding sites of ZSM-5 catalysts, the activation energy of desorption of dimethyl ether is the key descriptor over the active sites during the induction period of dimethyl ether conversion. Low activation energies of dimethyl ether desorption correlate with lower barriers of propylene formation during the induction period of propylene formation from dimethyl ether. Tuning the site properties, through the site density, is invaluable for improving the formation of propylene from methanol in the induction period. Tuning the surface characteristics, via the binding energies, is necessary to increasing propylene formation from dimethyl ether in the induction period.

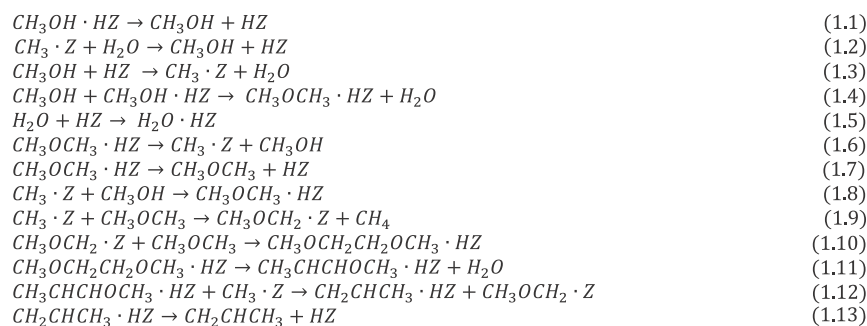
EXPERIMENTAL SECTION

Materials. The ammonium form of zeolites of different compositions (Si/Al ratio = 25, 36, 135) was pressed, crushed, and sieved to obtain particle sizes in the range of 250–500 μm . Ten milligrams of these zeolites, herein referred to as ZSM-5 (25), (36), and (135) were used. ZSM-5 (25) was purchased from Zeolyst International, while ZSM-5 (36) and ZSM-5 (135) catalysts were obtained from BP Chemicals. Anhydrous DME (99.999%) and argon (99.999%) were obtained from CK Special Gases Ltd. Ultrahigh purity water-free methanol (99.8%) was purchased from Sigma-Aldrich.

Temporal Analysis of Product (TAP) Reactor. The temperature-programmed surface reaction (TPSR) experiments were conducted in a temporal analysis of product (TAP) reactor. The zeolites were decomposed under vacuum conditions in the TAP reactor. A mixture of 5 vol % DME (balance argon) or 5 vol % methanol (balance argon) was fed into the TAP system using continuous feeding valves. The TAP reactor⁴⁵ in its standard configuration consists of three chambers in series: (a) the reactor chamber, (b) the differential chamber, and (c) the detector chamber. A short active catalyst bed of 2 mm packed bed in an overall bed length of 25 mm was housed in an inert quartz tube, which was placed in a metallic body to provide further mechanical stability.⁴⁶ The pressure at the inlet of the reactor chamber is ca. 1000 Pa under continuous flow. The pressure is 10^{-5} Pa at the exit of the reactor chamber. The pressure is 10^{-6} Pa at the end of the differential chamber, and the pressure in the detector chamber, where the quadrupole mass spectrometer (QMS) is housed, is 10^{-7} Pa.

Characterization. The characterization of the catalyst samples has been reported before.^{6,32} The morphological features of the fresh zeolite samples were characterized by using a Carl Zeiss sigma series field emission scanning electron microscope. The fresh samples were studied by X-ray diffraction (XRD) with a Bruker D5005 diffractometer using Cu K α radiation equipped with the standard Bragg–Brentano geometry and a diffracted beam graphite monochromator. Nitrogen physisorption studies were carried out on a Micromeritics 2020 unit. The samples were degassed by heating to 673 K under a vacuum (10^{-6} mbar) for 12 h. After degassing, the weight of the dried sample was determined and the sample was subsequently cooled to 77 K, and liquid nitrogen was adsorbed at increasing partial pressures.

The ZSM-5 (25) catalyst has a crystallite size of 0.10 ± 0.02 μm , an apparent BET surface area of $413 \text{ m}^2 \text{ g}^{-1}$, $428 \mu\text{mol g}^{-1}$ of Brønsted acid sites (BAS), $35 \mu\text{mol g}^{-1}$ of Lewis acid sites (LAS), and a BAS/LAS ratio of 12.2. The ZSM-5 (36) catalyst has a crystallite size of 0.33 ± 0.05 μm , an apparent BET surface area of $410 \text{ m}^2 \text{ g}^{-1}$, $117 \mu\text{mol g}^{-1}$ of Brønsted acid sites (BAS), $80 \mu\text{mol g}^{-1}$ of Lewis acid sites (LAS), and a BAS/LAS ratio of

Scheme 1. Pathway for the Formation of the First C–C Bond and Primary Olefins over the Brønsted Acid Sites (HZ) Present on ZSM-5 Catalysts


1.5. The ZSM-5 (135) catalyst has a crystallite size of $0.78 \pm 0.07 \mu\text{m}$, an apparent BET surface area of $358 \text{ m}^2 \text{ g}^{-1}$, $78 \mu\text{mol g}^{-1}$ of BAS, $30 \mu\text{mol g}^{-1}$ of LAS, and a BAS/LAS ratio of 2.6.^{6,32}

Temperature-Programmed Surface Reaction (TPSR) Studies. Before starting each experiment, the ammonium form of the zeolite catalyst was decomposed at 15 K min^{-1} from room temperature to 723 K and held for 30 min before cooling at 25 K min^{-1} to room temperature under vacuum conditions. Thereafter, a baseline argon flow was established over fresh and working ZSM-5 (25), ZSM-5 (36), and ZSM-5 (135) catalysts. The temperature-programmed surface reaction experiment was carried out by saturating the catalyst with $5 \text{ vol } \%$ of methanol (balance argon) or $5 \text{ vol } \%$ of dimethyl ether (balance argon) at $10^{-8} \text{ mol s}^{-1}$ and then subjecting the catalyst immediately to a linear temperature ramp of 15 K min^{-1} up until 723 K . A sample temperature-programmed surface reaction profile is given in our previous work⁴¹ as well as in Section S1 of the Supporting Information.

ZSM-5 catalysts, received from the manufacturer, decomposed without further modifications and subjected to advanced kinetic characterization using the TAP reactor are denoted in this work as fresh catalysts. In order to obtain working ZSM-5 catalysts, the ammonium form of the fresh ZSM-5 catalysts with Si/Al ratios of 25, 36, and 135 was calcined with $30\% \text{ O}_2/\text{N}_2$ in a fixed bed reactor of 4 mm I.D and 6 mm O.D at 10 K min^{-1} until 723 K and held there for 30 min before subsequently cooling at 25 K min^{-1} under nitrogen gas to 673 K , where they were subjected to $1.3 \text{ vol } \%$ of methanol at a flow rate of 10 mL min^{-1} . Gaseous products were monitored using an online GC-FID instrument equipped with an Equity-1 capillary column. Samples were withdrawn after 2 h of time-on-stream from the fixed bed reactor. The working catalysts were used as received from the atmospheric fixed bed reactor and subjected, without further modification, to decomposition and further kinetic tests in the TAP reactor.

During the TPSR experiments, the effluent was monitored using the QMS housed in the detector chamber of the TAP reactor. The response of the QMS was calibrated by passing continuous streams of various gases (methanol, dimethyl ether, water, ethylene, and propylene) in argon over an inert quartz bed with a particle diameter between 355 and $500 \mu\text{m}$. The inert quartz bed had a bed length similar to the active catalyst bed length used in the standard TPSR experiments. The sensitivity coefficients were obtained from the calibration data and used to obtain molar flow rates of the respective constituents. Argon was monitored at $m/e = 40$, CH_3OH at $m/e = 31$, CH_3OCH_3 at $m/e = 45$, H_2O at $m/e = 18$, C_2H_4 at $m/e = 27$, and C_3H_6 at $m/e = 41$. Previous methanol and DME step response work on ZSM-5

catalysts in our laboratory showed that ethylene and butene selectivities were negligible at 573 K under vacuum conditions. Subsequent deconvolution allowed for the subtraction of minor fragments of other species from the main species. The quantification procedure is detailed in Section S2 of the Supporting Information. The low base pressure, which is 10^{-7} Pa in the detector chamber, allows for the high detection sensitivity necessary for quantitative analysis. We observe no deactivation with time on stream over the ZSM-5 catalysts using similar molar flow rates and temperatures over our experimental time scale.⁶

COMPUTATIONAL METHODOLOGY

Microkinetic Modeling. A nonideal plug flow reactor model was used to simulate the temperature-programmed surface reaction experiments. This model accounts for adsorption, desorption, and surface reactions at the catalyst particle surface and dispersion and convection in the reactor. The nonideal plug flow reactor model was constructed using an in-house MATLAB code called MTOTAPCAT.⁴¹

As previously described in,⁴¹ although the temperature-programmed surface reaction at low pressures and high velocities is unlikely to be affected by dispersion, a second reactor dimension is required to account for the penetration of the zeolite pore system in the radial dimension. However, in an initial stage of code development, explicitly accounting for a 2D geometry profile in a transient kinetic problem involving many gaseous and surface species proved to be computationally expensive. A workaround strategy using an axial dispersion term only was considered. A particle-resolved transient kinetic study is outside the scope of this study.

The MTOTAPCAT code allows for the estimation of the pre-exponential factors and activation energies of desorption, reaction, and formation of primary olefins from methanol and dimethyl ether over fresh and working ZSM-5 catalysts. In the MTOTAPCAT code, desorption rate parameters are fitted and adsorption rates are calculated. Here, adsorption, desorption, and surface reaction rates can be extracted directly from the kinetic parameters.

A kinetic scheme based on a methoxy methyl pathway^{22,23} involving the methoxy methyl cation, dimethoxyethane, and methyl propenyl ether was used to describe the formation of primary olefins (Scheme 1). Previously, we showed that this pathway gives the closest agreement (in comparison to methane-formaldehyde, carbon monoxide, carbene routes) with transient kinetic data during the induction period of a step response cycle.^{40–42} This methoxy methyl pathway only accounts for the formation of the first C–C bond in the

induction period and does not consider a transition regime or steady-state period as decoupled previously⁶

Recently, we observed that two groups of adspecies desorb separately from ZSM-5 catalysts used for step response of dimethyl ether⁴⁰ conversion leading to steady state. Although the methoxy methyl pathway was observed over SAPO-34 catalysts²² and catalyst structure plays a major role in the product obtained,²⁹ this pathway over ZSM-5 catalysts would allow for mechanistic comparisons with the archived literature. The kinetic model was solved according to eqs 2 and 3. Assuming a first-order reversible process⁴⁷

Gas

$$\varepsilon_b \frac{\partial C_{i,g}}{\partial t} = D_{i,e} \frac{\partial^2 C_{i,g}}{\partial z^2} - u \frac{\partial C_{i,g}}{\partial z} - \Gamma_t S_v (1 - \varepsilon_b) (k_a c_i - k_d \theta_{iz}) \quad (2)$$

Surface

$$\frac{\partial \theta_i}{\partial t} = k_a c_i - k_d \theta_{iz} \quad (3)$$

where k_a is the adsorption coefficient ($\text{m}^3 \text{mol}^{-1} \text{s}^{-1}$), C_i is the concentration of the gas-phase component, i (mol m^{-3}), ε_b is the bed porosity (-), u is the superficial velocity (m s^{-1}), z is the bed length (m), t is time (s), Γ_t is the concentration of active sites per unit surface area of catalyst ($\text{mol m}_{\text{cat}}^{-2}$), S_v is the catalyst surface area per unit volume ($\text{m}_{\text{cat}}^{-1}$), k_d is the desorption rate coefficient (s^{-1}), θ_{iz} is the fractional surface coverage of the adsorbed species, and $D_{i,e}$ is the dispersion coefficient ($\text{m}^2 \text{s}^{-1}$).

This study is one of a series of studies^{6,32,39–44,48,49} to obtain mechanistic information on the formation of the primary C–C bond during the induction period of methanol and dimethyl ether conversion using the TAP reactor.

The dispersion coefficient $D_{i,e}$, bed porosity, and superficial velocity were fixed according to previous step response experiments⁴² conducted under similar conditions. The initial and boundary conditions are given below.

Methanol TPSR. Initial conditions

$$t = 0, C_{i,j} = C_{\text{MeOH},j}, C_{\text{Ar},j}, C_{\text{others}} = 0, \theta_i = 0 \text{ (except } \theta_{\text{MeOH}} = 1)$$

Boundary conditions

$$C_i(t, 0): C_{i,j} = C_{\text{MeOH},j}, C_{\text{Ar}}, C_{\text{others}} = 0, \\ \theta_{\text{MeOH},j} = 1, \theta_{\text{Ar},j} = 0, \theta_{\text{others}} = 0 \quad C_i(t, J): \frac{dC_{i,j}}{dt} = 0; \\ \frac{d\theta_{i,j}}{dt} = 0$$

DME TPSR. Initial conditions

$$t = 0, C_{i,j} = C_{\text{DME},j}, C_{\text{Ar},j}, C_{\text{others}} = 0, \theta_i = 0 \text{ (except } \theta_{\text{DME}} = 1)$$

Boundary conditions

$$C_i(t, 0): C_{i,j} = C_{\text{DME},j}, C_{\text{Ar}}, C_{\text{others}} = 0, \theta_{\text{DME},j} = 1, \\ \theta_{\text{Ar},j} = 0, \theta_{\text{others}} = 0 \quad C_i(t, J): \frac{dC_{i,j}}{dt} = 0; \frac{d\theta_{i,j}}{dt} = 0$$

It is important to note that we make no distinction between the coverage over fresh and working catalysts under the initial and boundary conditions. This is because both catalyst forms were presaturated with methanol or dimethyl ether before the start of the temperature-programmed surface reaction experiments. Furthermore, prior to the start of the temperature-programmed surface reaction experiments, both catalyst forms were decomposed under vacuum conditions. Backward differencing was applied to the convection term in the partial differential equation above. To ensure numerical stability, the Courant–Friedrichs–Lewy (CFL) condition⁵⁰ was satisfied

$$\text{CFL} = \left| a \frac{\Delta t}{\Delta z} \right| \leq 1 \quad (4)$$

where $a = u/\varepsilon_b$. The time domain was divided into 400,000 strips, and the space domain was divided into 5 strips. This led to a reduction in the computational time while maintaining the CFL criterion.

The sum-of-square error (SSE) between the experiment and model was obtained according to^{51,52}

$$\text{SSE} = \sum_{n=1}^{N_c} \sum_{m=1}^{N_d} w_{n,m} (Y_{n,m}^{\text{obs}} - Y_{n,m}^{\text{cal}})^2 \rightarrow \min \quad (5)$$

where

n is the component number

m is the observation number

N_c is the total number of components

N_d is the total number of observations

$W_{n,m}$ is the weighting factor of the m -th observation of component n

$Y_{n,m}^{\text{obs}}$ is the experimental data

$Y_{n,m}^{\text{cal}}$ is the model data

The initial parameter estimates were significantly improved by reducing the sum-of-square error between the model and experiment (eq 5). Parameter optimization, which minimizes the sum-of-square error using a “fminsearch” function, was carried out in the MTOTAPCAT code for over 150 h in each case. The “fminsearch” function uses a Nelder–Mead simplex algorithm as described by.⁵³ In eq 5, the weighing factors were calculated as⁵⁴

$$w_{n,m} = \frac{1}{\sum_{m=1}^{x_{\text{exp}}} Y_{n,m}} \quad (6)$$

where x_{exp} is the total number of experimental points. The expression allows the minority species in the reaction medium to have a higher weighting factor. After optimization, each parameter was checked and validated (along with the sensitivity analysis) for physical significance.

We considered five gaseous species (methanol, dimethyl ether, water, ethylene, and propylene) and eight surface species (adsorbed methanol, adsorbed dimethyl ether, adsorbed water, surface methoxy species, methoxy methyl species, methyl propenyl ether, adsorbed dimethoxyethane, and adsorbed propylene) in this reduced model. However, there are >90 species including isomers formed in the hydrocarbon pool. Considering all elementary reactants and products under transient conditions is a formidable task, even on modern workstations. High computational costs and time required for the solution of coupled partial differential equations allowed for a focus on the transformation of major reactants and products.

Focusing on the induction period allows the consideration of a smaller number of species.

Sensitivity Analysis. Each parameter was multiplied by a perturbation factor, while the other rate parameters were kept constant to assess site-specific information on activity promoters and inhibitors during the temperature-programmed surface reaction of methanol and dimethyl ether over ZSM-5 catalysts. The relative changes in temperature-programmed surface reaction profiles were obtained with or without the perturbation factor. Subsequently, the sensitivity coefficient was obtained as given in eq 7

$$K_s = \frac{\ln(Y_p/Y_o)}{\ln(F)} \quad (7)$$

where Y_p and Y_o are the rates with and without perturbation respectively, and F is the perturbation factor. A perturbation factor of 0.2 was used during the temperature-programmed surface reaction of methanol. A perturbation factor of 0.2 was used during the temperature-programmed surface reaction of dimethyl ether, except for the low-temperature active sites, which showed exceptionally high sensitivity.⁴¹

Site-Specific Scaling Relations. Scaling relations were extracted by correlating the desorption energies of dimethyl ether ($E_{d,DME}$, kJ mol⁻¹) with the reaction energies of methoxy methyl and methyl propenyl ether ($\Delta E_{intermediate}$, kJ mol⁻¹) over fresh and working ZSM-5 catalysts as conducted in our previous work over ZSM-5 (36) and (135) catalysts.^{40,41} The approach was extended to the temperature-programmed surface reaction of dimethyl ether over ZSM-5 (25) catalysts. Further scaling relations were extracted by correlating the desorption energies of dimethyl ether with the reaction energies of propylene formation ($E_{propylene}$, kJ mol⁻¹).

Scaling relations were observed during the temperature-programmed surface reaction of methanol over ZSM-5 (25), (36), and (135) catalysts. Site-specific-scaling relations were also obtained by correlating the acid site density (ρ_{H^+} , mol g⁻¹) with the desorption energies of dimethyl ether ($E_{d,DME}$, kJ mol⁻¹) and desorption energies of methanol ($E_{d,MeOH}$, kJ mol⁻¹) for fresh and working ZSM-5 catalysts. The acid site density is also correlated with the reaction energies of methoxy methyl cation, methyl propenyl ether, and propylene formed over ZSM-5 catalysts. The density of acid sites ρ_{H^+} (mol g⁻¹) was obtained for each site ensemble. The average distance between acid sites, d_{ave,H^+-H^+} , can be obtained from the acid site density with information about the surface area of the zeolite catalysts by nitrogen physisorption and the effective area around the surface site taken for simplicity as a circle with the diameter equal to d_{ave,H^+-H^+} eq 8^{55,56}

$$d_{ave,H^+-H^+} = \sqrt{\frac{4S_{N_2}}{\pi\rho_{H^+}N_A}} \quad (8)$$

where S_{N_2} is the BET surface area (m² g⁻¹), and N_A is the Avogadro number, mol⁻¹.

RESULTS

Temperature-Programmed Surface Reaction Profile Analysis. Profiles of the temperature-programmed surface reaction of methanol and dimethyl ether over fresh and working ZSM-5 catalysts are given in Section S3 of the [Supporting Information](#). During TPSR of methanol over fresh ZSM-5 (25) catalysts, DME forms at ca. 473 K and propylene at ca. 668 K.

During the room-temperature adsorption of methanol on the ZSM-5 catalyst, room-temperature methoxylation occurs with increased water formation at ca. 328 K. There is no ethylene formation over fresh ZSM-5 (25) catalysts. During TPSR of methanol over working ZSM-5 (25) catalysts, DME forms at ca. 453 K and propylene at ca. 633 K, and room-temperature methoxylation occurs during methanol adsorption with increased water formation at 308 K.

During the temperature-programmed surface reaction of methanol over fresh ZSM-5 (36) catalysts, DME forms at ca. 473 K and propylene at ca. 653 K, with room-temperature methoxylation leading to the formation of water occurring during the adsorption phase and increased water formation at 303 K. There is no ethylene formation during the temperature-programmed surface reaction of methanol over fresh ZSM-5 (36) catalysts. During the temperature-programmed surface reaction of methanol over working ZSM-5 (36) catalysts, DME forms at ca. 473 K and propylene at ca. 698 K, with room-temperature methoxylation leading to the formation of water occurring during the adsorption phase and increased water formation at 318 K. There is no ethylene formation during the temperature-programmed surface reaction of methanol over working ZSM-5 (36) catalysts.

During the temperature-programmed surface reaction of methanol over fresh ZSM-5 (135) catalysts, DME forms at ca. 488 K; room-temperature methoxylation leading to water formation occurs immediately at 300 K. There is increased water formation at 313 K. Late propylene formation occurs at ca. 693 K. There is no ethylene formation over fresh ZSM-5 (135) catalysts. During the temperature-programmed surface reaction of methanol over working ZSM-5 (135) catalysts, DME forms at ca. 473 K; room-temperature methoxylation occurs with immediate formation of water during the methanol adsorption phase. There is increased water formation at 313 K. There is neither ethylene nor propylene formation during the temperature-programmed surface reaction of dimethyl ether over working ZSM-5 (135) catalysts (Table 1).

Table 1. Induction Period of Specie Formation during the TPSR of Methanol over ZSM-5 Catalysts

onset of specie formation, min	fresh ZSM-5 (25)	working ZSM-5 (25)	fresh ZSM-5 (36)	working ZSM-5 (36)	fresh ZSM-5 (135)	working ZSM-5 (135)
DME	11.5	10.2	11.5	11.5	12.5	11.5
water ^a	1.9	0	0	1.2	~1	~1
ethylene	—	—	—	—	—	—
propylene	24.5	22.2	23.5	26.5	26.2	—

^aRoom-temperature methoxylation (RTM) occurs; values refer to increased water formation above RTM values.

These induction temperatures were converted to induction times using a heating rate of 15 K min⁻¹ at a starting room temperature of 300 K (Table 1). In general, the induction times increase as Si/Al ratios increase. There is no induction time for water formation during the induction period of methanol conversion due to room-temperature methoxylation. Water forms instantaneously during the temperature-programmed surface reaction of methanol. After this, dimethyl ether and propylene form. There is no ethylene formation.

During TPSR of dimethyl ether over fresh ZSM-5 (25) catalysts, propylene forms at ca. 623 K, while methanol forms at ca. 528 K and water forms at ca. 353 K. During TPSR of dimethyl

ether over working ZSM-5 (25) catalysts, propylene forms at ca. 618 K, while methanol forms at ca. 513 K and water forms at ca. 373 K. Over ZSM-5 (25) catalysts during the temperature-programmed surface reaction of dimethyl ether, there is no ethylene formation. There is low-temperature olefin (ethylene and propylene) consumption between 473 and 593 K during the temperature-programmed surface reaction of dimethyl ether over fresh and working ZSM-5 (25) catalysts.

Methanol forms at ca. 523 K and propylene forms at ca. 653 K, and there is a low-temperature (303–453 K) water release that continues to increase during the temperature-programmed surface reaction of dimethyl ether over fresh ZSM-5 (36) catalysts. Methanol forms at ca. 493 K, propylene forms at ca. 653 K, and water forms at ca. 483 K during the temperature-programmed surface reaction of dimethyl ether over working ZSM-5 (36) catalysts. There is no ethylene formation over ZSM-5 (36) catalysts during the temperature-programmed surface reaction of dimethyl ether. There is a low-temperature olefin (ethylene and propylene) consumption between 453 and 593 K during the temperature-programmed surface reaction of dimethyl ether over fresh and working ZSM-5 (36) catalysts.

During the temperature-programmed surface reaction of dimethyl ether over fresh ZSM-5 (135) catalysts, methanol forms at ca. 573 K, water forms at ca. 353 K, and there is no propylene formation within the temperature range of 300–723 at 15 K min⁻¹. Over working ZSM-5 (135) catalysts, methanol forms at ca. 493 K, water forms at ca. 493 K, and there is no ethylene or propylene formation within the temperature range of 300–723 at 15 K min⁻¹ during the temperature-programmed surface reaction of dimethyl ether. There is a low-temperature olefin (ethylene and propylene) consumption between 453 and 593 K during the temperature-programmed surface reaction of dimethyl ether over fresh and working ZSM-5 (135) catalysts (Table 2).

Table 2. Induction Period of Specie Formation during the TPSR of DME over ZSM-5 Catalysts

onset of specie formation, min	fresh ZSM-5 (25)	working ZSM-5 (25)	fresh ZSM-5 (36)	working ZSM-5 (36)	fresh ZSM-5 (135)	working ZSM-5 (135)
methanol	15.2	14.2	14.9	12.9	18.2	12.9
water	3.5	4.9	0	12.2	3.5	12.9
ethylene	—	—	—	—	—	—
propylene	21.5	21.2	23.5	23.5	—	—

The induction temperatures were converted to induction times by using a heating rate of 15 K min⁻¹ using a starting room temperature of 300 K (Table 2). In general, the induction times increase as Si/Al ratios increase. In contrast to the temperature-programmed surface reaction of methanol, there is an induction period in the formation of water during the temperature-programmed surface reaction of dimethyl ether. The induction time of methanol formation during the temperature-programmed surface reaction of dimethyl ether is higher than the induction time of dimethyl ether formation during the temperature-programmed surface reaction of methanol. The induction times of propylene formation are lower during the temperature-programmed surface reaction of dimethyl ether compared to that of methanol.

Interestingly, over ZSM-5 (25) catalysts, we observed an induction period of 44 min during the conversion of dimethyl ether to olefins at 300 °C using a step response methodology in

the TAP reactor.⁴² Over the same catalysts and similar flow rates, using a temperature-programmed surface reaction methodology with dimethyl ether, an induction period of ca. 22 min is obtained. There are two major differences between prior step response experiments and the temperature-programmed surface reaction experiments. First, the catalyst was saturated with dimethyl ether during temperature-programmed surface reaction experiments, whereas the catalyst pores are empty during step response experiments. Second, during step response experiments, only binding and active sites lower than 573 K are activated; however, during DME TPSR experiments, binding and active sites up to 723 K are activated. As a result, a longer induction period is obtained during the step response experiments. We observe that the low-temperature active site is dominant (450–600 K) during the temperature-programmed surface reaction of dimethyl ether^{40,41,49} and a step response temperature of 573 K does not allow for the full functionality of the activation temperature of the dominant active site.

During the temperature-programmed desorption of methanol and dimethyl ether over ZSM-5 catalysts, we uncovered three adsorption site ensembles (low temperature: LT, medium temperature: MT, high temperature: HT) over ZSM-5 (25) and ZSM-5 (36) catalysts and two adsorption site ensembles over ZSM-5 (135) catalysts.³² Six ensembles of sites are required for the adsorption, desorption, and surface reaction of methanol and dimethyl ether over ZSM-5 catalysts.^{40,41} Of these six site ensembles, three are binding sites associated with adsorption and desorption, and three are active sites that are associated with adsorption, desorption, and reactions leading to propylene formation. Altogether, there are low-temperature, medium-temperature, and high-temperature binding sites and low-temperature, medium-temperature, and high-temperature active sites.

We observe substantial differences between TPSR profiles of methanol and dimethyl ether over ZSM-5 catalysts of different compositions. In our previous work,⁴¹ we observed that site 4, i.e., the low-temperature active site ensemble, has a large number of significant chemical steps during the temperature-programmed surface reaction of dimethyl ether over fresh and working ZSM-5 (36) catalysts. Similar behavior can be observed over fresh and working ZSM-5 (25) catalysts (Figure 1 and Section S4 of the Supporting Information). During the temperature-programmed surface reaction of methanol over ZSM-5 catalysts, we observe that the low-temperature, medium-temperature, and high-temperature binding sites are the dominant site ensembles during the induction period. This can also be readily identified by the position of the bulge in the TPSR profiles. For the temperature-programmed surface reaction of methanol, the largest bulge is between 300 and 450 K, while for the temperature-programmed surface reaction of dimethyl ether, the largest bulge is between 450 and 600 K (Figure 1).

The effect of using working catalysts during TPSR studies over ZSM-5 catalysts is much more pronounced with methanol than with dimethyl ether. During the temperature-programmed surface reaction of dimethyl ether, there is a negligible influence of changing the catalyst state from a fresh state to a working catalyst state. However, during the temperature-programmed surface reaction of methanol, the influence of the catalyst state is higher (Figure 2 and Section S5 of the Supporting Information). During the temperature-programmed surface reaction of

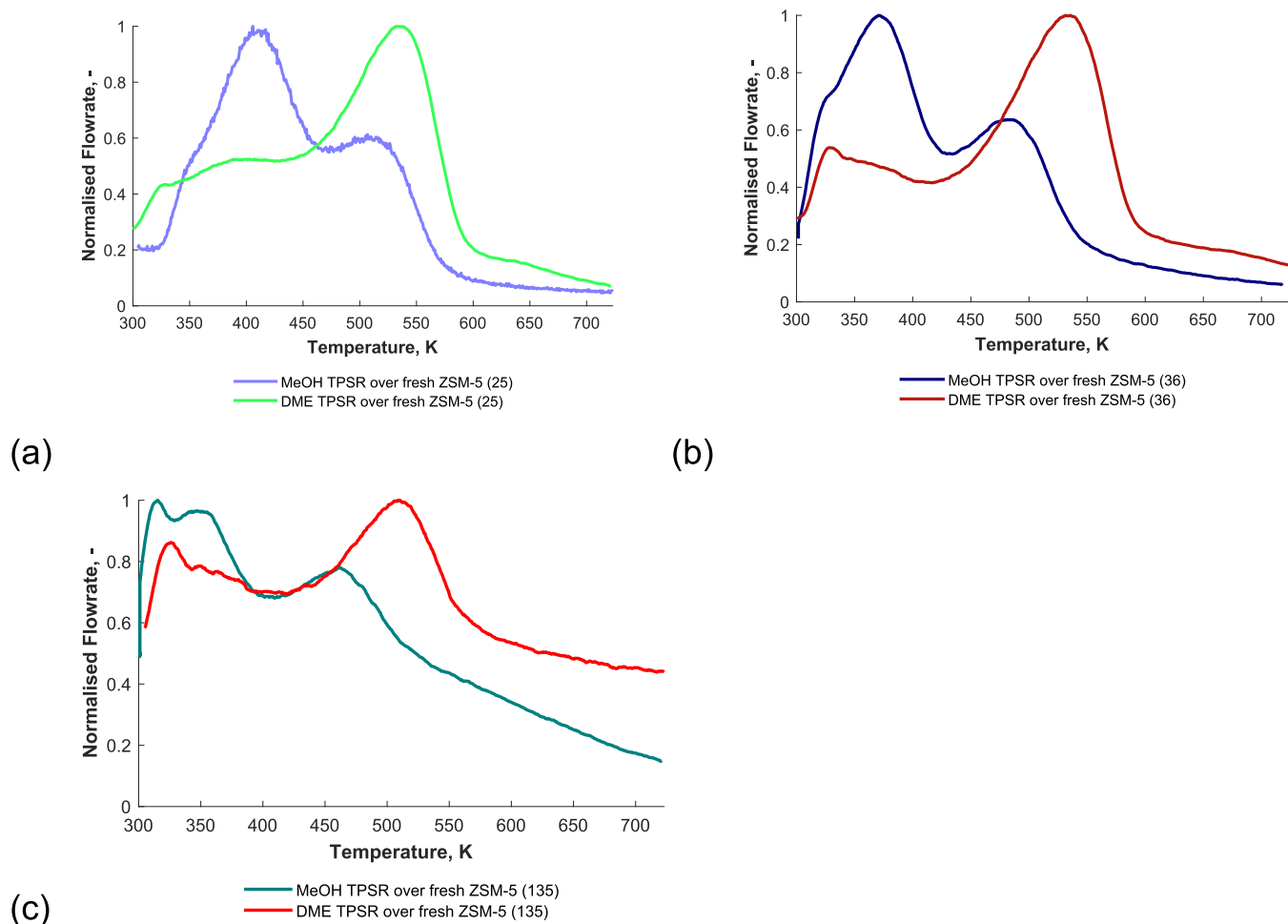


Figure 1. Comparison between methanol TPSR and dimethyl ether TPSR profiles over fresh and working ZSM-5 catalysts of the Si/Al ratio of (a) 25, (b) 36, and (c) 135.

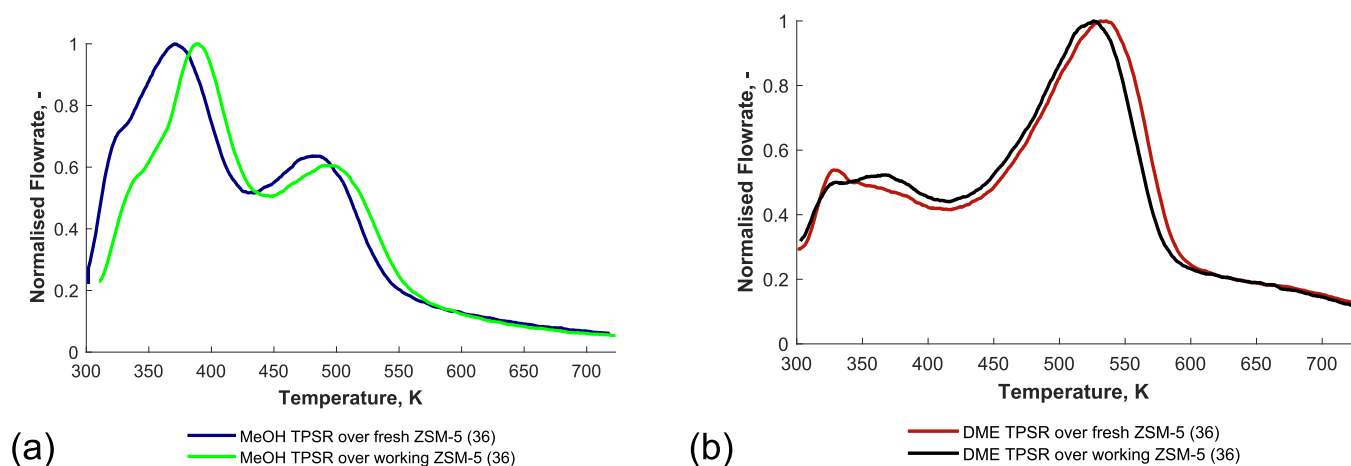


Figure 2. Comparison of fresh to working ZSM-5 catalysts of Si/Al = 36 during the temperature-programmed surface reaction of (a) methanol and (b) dimethyl ether.

methanol, barriers are generally shifted to the right over working catalysts in comparison to those of fresh catalysts.

Generally, the Si/Al ratio has an impact on the evolution of products during the temperature-programmed surface reaction of methanol and dimethyl ether over ZSM-5 catalysts. We showed in Tables 1 and 2 that with an increase in Si/Al ratios, the induction times of methanol, water, and propylene during

DME TPSR and of dimethyl ether, water, and propylene during methanol TPSR increase. We observe that with an increase in the Si/Al ratio during the temperature-programmed surface reaction of methanol, the evolution of the methanol profile shifts to the left (Figure 3 and Section S6 of the Supporting Information) over fresh and working ZSM-5 catalysts. During the temperature-programmed surface reaction of dimethyl

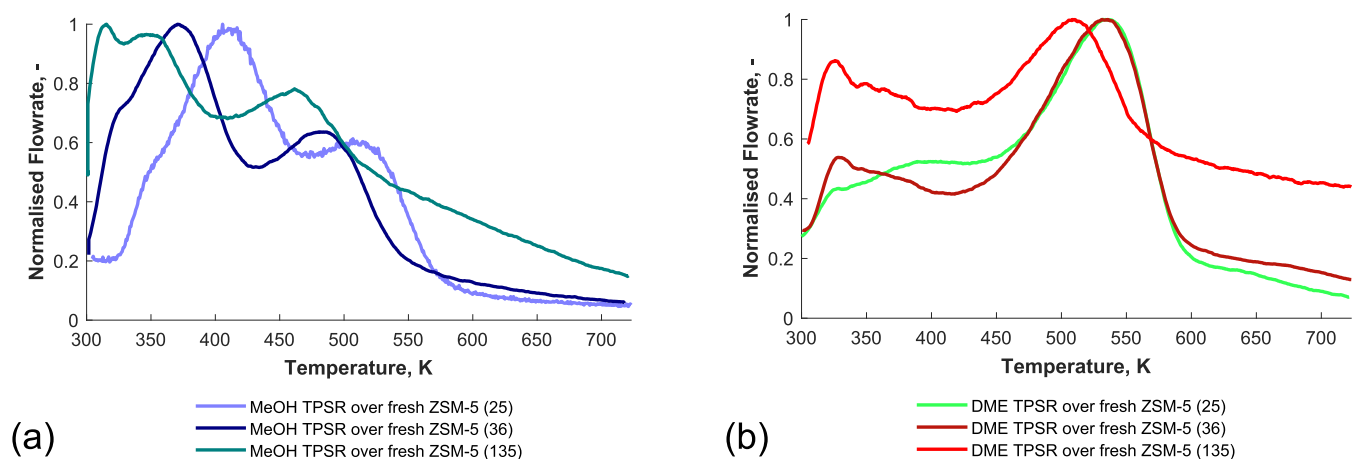


Figure 3. Comparison between ZSM-5 (25), (36), and (135) catalysts during the temperature-programmed surface reaction of (a) methanol and (b) dimethyl ether.

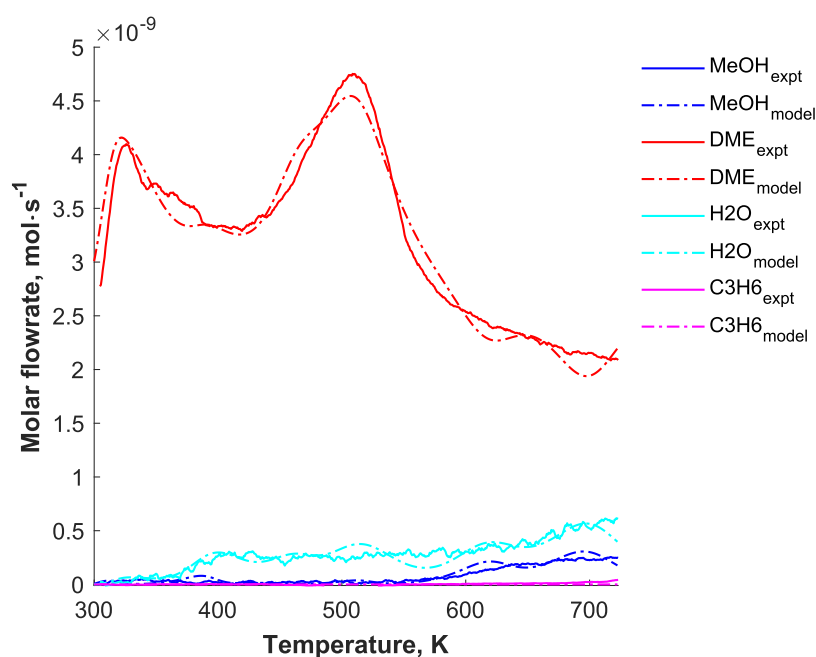


Figure 4. TPSR experiments with 5 vol % of DME inlet feed over fresh ZSM-5 (135) catalysts. Reproduced with permission from ref 41. Copyright 2021 Elsevier.

ether, a similar behavior is observed over fresh ZSM-5 catalysts. However, there is little or negligible influence of the Si/Al ratio during the temperature-programmed surface reaction of dimethyl ether over working catalysts.

In summary, with an increase in the Si/Al ratio, the induction period of dimethyl ether and propylene formation increases for the temperature-programmed surface reaction of methanol during which the methanol profiles shift to the left over fresh and working ZSM-5 catalysts. The induction period of methanol, water, and propylene formation increases with Si/Al ratio for the temperature-programmed surface reaction of dimethyl ether, while the dimethyl ether profiles shift to the left for fresh catalysts and hardly change for working catalysts.

Experiments are compared to the microkinetic model using a 1D transient heterogeneous reactor model during the temperature-programmed surface reaction of methanol and dimethyl ether (Figures 4–9 and Section S7 of the Supporting Information). The extracted kinetic parameters and site

densities are given in Sections S8–S13 of the Supporting Information. There is good agreement between the model and experimental data. The kinetic model should predict the concentration profiles of methanol, dimethyl ether, water, and propylene simultaneously. Given six site ensembles, this requires the optimization of up to 78 rate constants (Scheme 1). The kinetic model can predict the formation of methanol, DME, and propylene over the ZSM-5 catalysts very well. There is a fair agreement between the experimental and model simulations of water during the temperature-programmed surface reaction of methanol over the ZSM-5 (25) and ZSM-5 (36) catalysts. Inclusion of many more chemical steps in the microkinetic model can bring further agreement with the transient kinetic data. However, a balance was struck between the need to increase the number of parameters (and hence chemical steps in each site ensemble) and computational time required for transient kinetic simulations, especially in the optimization routine. Nonetheless, in many cases, the sum-of-square error

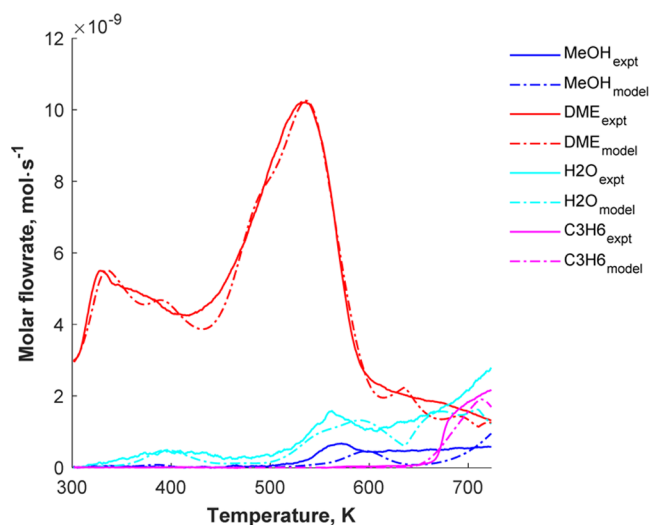


Figure 5. TPSR experiments with 5 vol % of DME inlet feed over fresh ZSM-5 (36) catalysts. Reproduced with permission from ref 41. Copyright 2021 Elsevier.

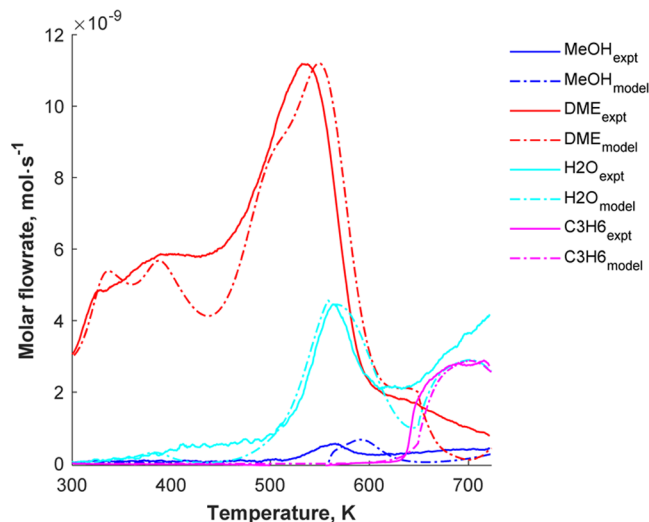


Figure 6. TPSR experiments with 5 vol % of DME inlet feed over fresh ZSM-5 (25) catalysts.

was reduced by 2 orders of magnitude from the initial parameter estimates. Inclusion of anomalous diffusion in a particle-resolved transient reactor model can help to bring further agreement with experimental data. However, this is outside the scope of this study.

Adsorption steps are nonactivated. Generally, barriers increase from the low-temperature binding sites to the high-temperature active sites over each ZSM-5 catalyst. Within each site ensemble, barriers generally increase from the initial steps, which are the molecular and dissociative adsorption of methanol and dimethyl ether to the formation of propylene. The induction period of propylene formation is regulated by the energetics of the formation of stable intermediates, such as the methoxy methyl cation, dimethoxyethane, and methyl propenyl ether. An increase in pre-exponential factors shifts the model profiles to the left, while an increase in activation energies shifts the model profiles to the right. An increase in site densities shifts the profile upward or downward to fit the experimental TPSR profiles.

DISCUSSION

Comparison of the Temperature-Programmed Surface Reaction of Methanol to Dimethyl Ether. In our previous work, we observed that the formation of olefins can be grouped into three stages:⁶ induction period, transition regime, and steady state. We observed that not all species achieve steady state simultaneously and during the steady-state stage, two groups of adspecies are adsorbed on the ZSM-5 catalyst surface.^{6,40} Overall, hundreds of species including isomers are produced during the formation of the hydrocarbon pool from methanol and dimethyl ether. During the temperature-programmed surface reaction of methanol and dimethyl ether over ZSM-5 catalysts, we focused on the induction period alone as this limits the number of chemical steps involved. We did not include any isomers in our analysis.

In comparison to dimethyl ether, extra chemical steps are included in the simulation of the temperature-programmed surface reaction of methanol over ZSM-5 catalysts. In the case of the temperature-programmed surface reaction of methanol, the starting catalyst state over fresh and working ZSM-5 catalysts is the adsorbed methanol. In the first step, adsorbed methanol desorbs molecularly, leading to $\text{CH}_3\text{OH}_{(g)}$ and a free active site (reaction 1.1 of Scheme 1), whereas, for the temperature-programmed surface reaction of dimethyl ether, the starting catalyst state over fresh and working ZSM-5 catalysts is the adsorbed dimethyl ether. The first step is where the adsorbed dimethyl ether desorbs molecularly to $\text{DME}_{(g)}$ and a free active site (reaction 1.7 of Scheme 1). During the temperature-programmed surface reaction of methanol, much more water is formed due to room-temperature methoxylation.^{57,58} Consequently, it was necessary to include the formation of adsorbed dimethyl ether and $\text{H}_2\text{O}_{(g)}$ from methanol (reaction 1.4 of Scheme 1). The release of water is also regulated during the temperature-programmed surface reaction of methanol by the adsorption of water (reaction 1.5 of Scheme 1), room-temperature methoxylation (reactions 1.2 and 1.3), and the formation of methyl propenyl ether (reaction 1.11 of Scheme 1).

In our previous work on the temperature-programmed desorption of methanol and dimethyl ether over fresh and working ZSM-5 catalysts,³² we observed that the adsorption stoichiometry is higher over methanol compared to dimethyl ether. This means that more methanol molecules are adsorbed per binding site compared to adsorbed dimethyl ether molecules per binding site. Similarly, in this work, we observe that more methanol molecules adsorb per binding site and per active site during the temperature-programmed surface reaction of methanol compared to dimethyl ether over fresh and working ZSM-5 catalysts.

Finally, we show later that during the temperature-programmed surface reaction of dimethyl ether over fresh and working catalysts, the low-temperature active site ensemble (activated between 450 and 600 K) is dominant.⁴¹ However, during the temperature-programmed surface reaction of methanol, the low-temperature, medium-temperature, and high-temperature binding site ensembles (activated between 300 and 450 K) are dominant. In fact, more binding sites are involved during the induction period of methanol conversion to olefins over zeolite catalysts. During the induction period of the conversion of dimethyl ether to olefins, more active sites are involved. In this analysis, binding sites do not lead to the formation of propylene, but active sites do.

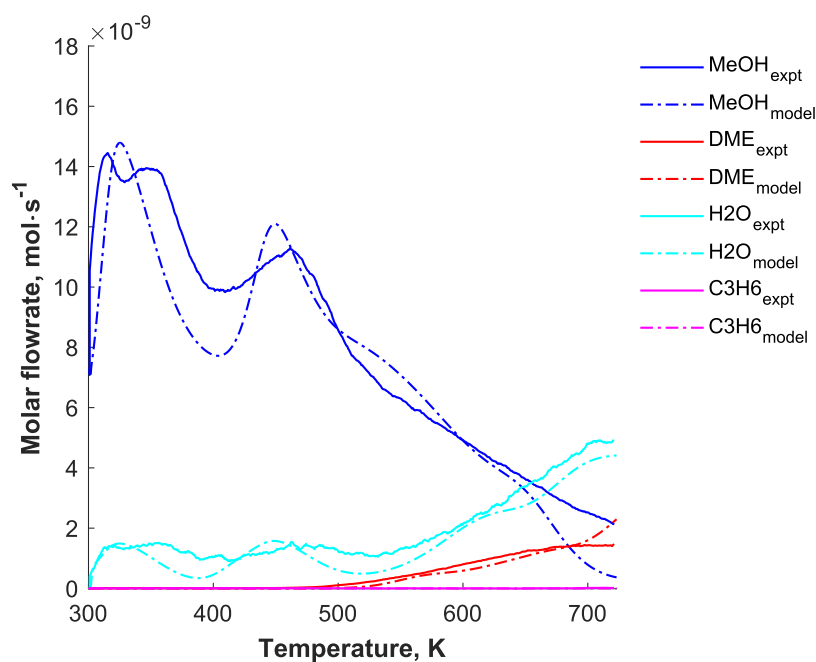


Figure 7. TPSR experiments with 5 vol % of methanol inlet feed over fresh ZSM-5 (135) catalysts.

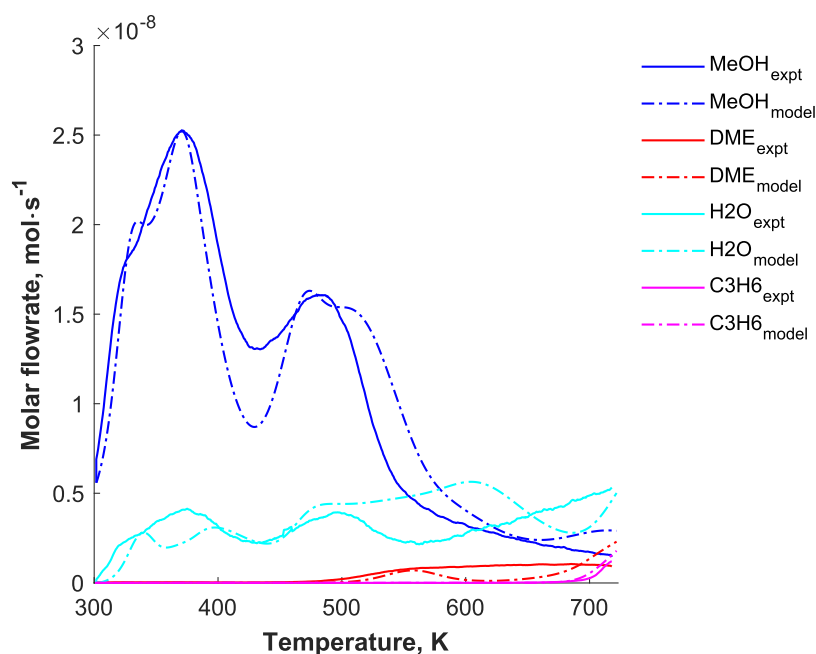


Figure 8. TPSR experiments with 5 vol % of methanol inlet feed over fresh ZSM-5 (36) catalysts.

Comparison of Fresh to Working Catalysts. The temperature-programmed surface reaction of methanol and dimethyl ether was studied during the induction period over fresh ZSM-5 catalysts as the catalyst state changes from a fresh state to a working state and adspecies are occluded onto the catalyst. Over working ZSM-5 catalysts, the induction period was studied as the catalyst evolves from one working state to another working state. During the experimental study, fresh and working catalysts were pretreated before temperature-programmed surface reaction studies (Section 3). The fresh or working ZSM-5 catalysts of different compositions were then saturated with methanol or dimethyl ether. In the TPSR model, the starting catalyst state for the temperature-programmed

surface reaction of methanol and dimethyl ether is adsorbed methanol and adsorbed dimethyl ether, respectively. Barriers are generally higher over working catalysts compared with that of fresh catalysts. Adspecies formation competes with occluded species in the working catalysts for active sites. As a result, more energy is expended in the binding and reaction of species on the catalyst.

Reductionist and Integrated Approach to MTO Catalysis. We used two approaches to study the conversion of methanol to olefins over ZSM-5 catalysts. These are the reductionist and integrated approaches. While the integrated approach attacks a scientific problem in its entire complexity, the reductionist approach ensures the breakdown of such complex

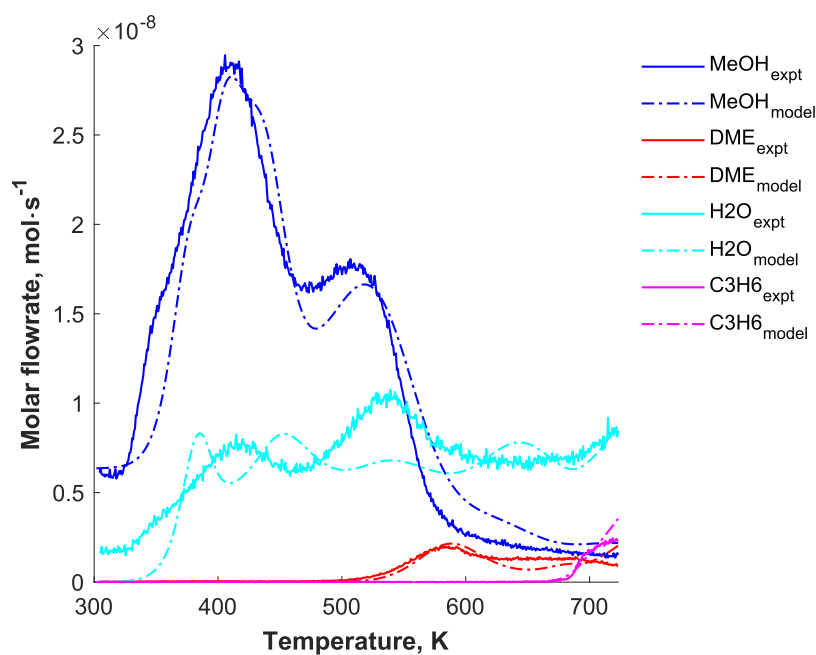


Figure 9. TPSR experiments with 5 vol % of methanol inlet feed over fresh ZSM-5 (25) catalysts.

problem into reducible bits. The challenge lies in understanding whether the sum of the reducible bits can reproduce a problem in its whole complexity. Using the reductionist approach, we attempt to break down the complex process that occurs as structural changes to the active sites ensue, and the hydrocarbon pool forms during the induction period of the conversion of methanol to olefins. First, we compared the desorption of methanol to dimethyl ether over fresh and working catalysts.³² We observed that dimethyl ether desorbs at higher temperatures and requires a higher activation energy of desorption compared to methanol. Dimethyl ether was then used to study the induction period of propylene formation using step response cycles.⁴² A 44 min induction period was observed at 300 °C leading to the formation of propylene as the primary olefin. Thereafter, we studied the competitive adsorption of oxygenates (methanol, dimethyl ether) and aromatics (toluene, diphenyl-ethane) over ZSM-5 catalysts.³⁹ The competitive adsorption analyses and experiments show that dimethyl ether stays on the catalyst surface much longer. A further rationale for this study was the evidence in the archived literature of impurities as organic precursors for olefin formation over ZSM-5 catalysts.⁵⁹ Overall, dimethyl ether requires higher activation energies of desorption and higher temperatures to desorb from the catalyst surface. We then compared precursors of the direct mechanism (dimethoxymethane, carbon monoxide, hydrogen) to the indirect mechanism (1,5-hexadiene) for their effect on the induction period and transition regime of the formation of primary olefins from dimethyl ether.⁶ We observed that the direct precursors reduced the induction period of primary olefin formation while accelerating the transition regime. However, while the indirect precursors reduced the induction period, they decelerated the rate at which steady state was reached due to their competitive adsorption with the dimethyl ether over the ZSM-5 catalysts.

The diffusion of methanol, dimethyl ether, and water does not limit the conversion of methanol and dimethyl ether over ZSM-5 catalysts.^{43,44} At room temperature in ZSM-5 (36) catalysts, isotropic methanol rotation (rotational diffusion coefficient, D_R

$= 2.6 \times 10^{10} \text{ s}^{-1}$) was observed, which is in contrast to diffusion confined to a sphere matching the 5.5 Å channel width in ZSM-5 (135) catalysts, suggesting that motion is more constrained in the lower Si/Al catalyst. At higher temperatures, confined methanol diffusion is exhibited in both ZSM-5 (36) catalysts and ZSM-5 (135) catalysts with self-diffusion coefficients in the range of $8\text{--}9 \times 10^{-10} \text{ m}^2 \text{ s}^{-1}$. The activation energy of methanol diffusion obtained in ZSM-5 (135) catalysts is 0.58 kJ mol^{-1} . An activation energy of methanol diffusion could not be obtained for the ZSM-5 (36) catalysts. For dimethyl ether, diffusion confined to a sphere at all temperatures is observed in both catalysts with self-diffusion coefficients in the range of $9\text{--}11 \times 10^{-10} \text{ m}^2 \text{ s}^{-1}$. The larger self-diffusion coefficient obtained for dimethyl ether arises from the sphere of confinement being larger in ZSM-5 (36) catalysts, which is 6.2 Å in diameter compared to the 5.5 Å pore channel width, suggesting that mobile dimethyl ether is sited in the channel intersections, in contrast to mobile methanol, which is sited in the channels. The activation energy of dimethyl ether diffusion obtained for ZSM-5 (36) catalysts and ZSM-5 (135) catalysts, respectively, is 0.96 and 1.33 kJ mol^{-1} . ZSM-5 (36) and (135) catalysts were loaded with ca. 12 wt % of methanol or dimethyl ether.⁴³ QENS measurements probed water confined in ZSM-5 samples with Si/Al ratios of 15, 40, and 140 at 2.8 wt % of loading.⁴⁴ In the lower silica sample, water diffusion was confined to a sphere (with radii ranging from 3.4 to 4.3 Å), suggesting that mobile water was located within the ZSM-5 channels with self-diffusion coefficient of $\sim 0.9\text{--}1.8 \times 10^{-9} \text{ m}^2 \text{ s}^{-1}$. In the high silica zeolite, the diffusion was observed to be far less confined and more long-ranged in nature with self-diffusion coefficients of $\sim 1.8\text{--}4.8 \times 10^{-9} \text{ m}^2 \text{ s}^{-1}$. The activation energy of water diffusion ranged from ~ 19 to 23 kJ mol^{-1} .

Then, the induction period of the conversion of dimethyl ether to olefins was studied using a combination of the temperature-programmed surface reaction and microkinetic modeling. We observed that the desorption of dimethyl ether was still higher than the desorption energy of methanol over ZSM-5 catalysts. Site-specific scaling relations between the

Table 3. Proportion of Binding and Active Sites during the Induction Period of Methanol Conversion over ZSM-5 Catalysts

	ZSM-5 (25)		ZSM-5 (36)	
	fresh	working	fresh	working
binding (mol g ⁻¹)	2.53 × 10 ⁻⁶	3.60 × 10 ⁻⁶	2.35 × 10 ⁻⁶	2.42 × 10 ⁻⁶
active (mol g ⁻¹)	1.69 × 10 ⁻⁶	1.01 × 10 ⁻⁶	1.15 × 10 ⁻⁶	9.92 × 10 ⁻⁷
binding/total	60.0%	78.1%	67.1%	70.9%

Table 4. Proportion of Binding and Active Sites during the Induction Period of Dimethyl Ether Conversion over ZSM-5 Catalysts

	ZSM-5 (25)		ZSM-5 (36)	
	fresh	working	fresh	working
binding (mol g ⁻¹)	4.14 × 10 ⁻⁷	5.60 × 10 ⁻⁷	3.22 × 10 ⁻⁷	3.40 × 10 ⁻⁷
active (mol g ⁻¹)	6.99 × 10 ⁻⁷	1.64 × 10 ⁻⁶	6.56 × 10 ⁻⁷	6.15 × 10 ⁻⁷
binding/total	37.2%	25.5%	32.9%	35.6%

desorption energy of dimethyl ether and the reaction energies of the intermediates were observed. We observe propylene as the primary and major olefin over the ZSM-5 catalysts. The desorption energy of dimethyl ether was identified as a descriptor for catalyst design.^{40,41} This temperature-programmed surface reaction of dimethyl ether shows the low-temperature active site as the dominant site during the induction period.

In the aforementioned work, we used the reductionist approach to break down the induction period of methanol conversion into adsorption and desorption,³² competitive adsorption,^{6,39} diffusion,^{43,44} and reaction.^{40–42} In this work, we have used the integrated approach, where we study the induction period of the conversion of methanol to primary olefins over fresh and working catalysts as a whole. Although propylene is still the primary olefin formed during the temperature-programmed surface reaction of methanol, the dominant sites of the induction period are the low-temperature, medium-temperature, and high-temperature binding sites due to water adsorption and desorption. Whereas catalyst development should focus on sites activated between 300 and 450 K for methanol conversion, the sites activated between 450 and 600 K should be considered for dimethyl ether conversion. Another significant difference is that the reductionist approach would not allow for consideration of the copious amount of water formed during the induction period of methanol conversion. As shown later, there are also significant differences in the number of adsorbed molecules/per binding (or active) site and the distance between acid sites during the temperature-programmed surface reaction of methanol and dimethyl ether over ZSM-5 catalysts.

Nature of Binding and Active Sites. 0.28, 0.84, and 0.31% of the overall sites are used in the transformation of dimethyl ether on fresh ZSM-5 (135), ZSM-5 (36), and ZSM-5 (25) catalysts. 0.32, 0.82, and 0.62% of the overall sites are used in the transformation of dimethyl ether over working ZSM-5 (135), ZSM-5 (36), and ZSM-5 (25) catalysts. During methanol transformation over fresh ZSM-5 (135), ZSM-5 (36), and ZSM-5 (25) catalysts, 1.48, 3, and 1.19% of the overall sites are used. Over working ZSM-5 (135), ZSM-5 (36), and ZSM-5 (25) catalysts, 0.95, 2.92, and 1.29% of the overall sites are used. During the temperature-programmed surface reaction of methanol and dimethyl ether, a higher site density is required for ZSM-5 (36) catalysts in comparison to that of ZSM-5 (135) and ZSM-5 (25) catalysts.

We characterized the acid sites according to binding sites and active sites. Binding sites are involved in species adsorption, species desorption, and the formation of intermediates.

However, binding sites do not possess the sufficient energy to form propylene. Active sites cover the whole spectrum including the adsorption, desorption, and reaction of species leading to propylene formation. Consequently, binding sites cover the earlier parts of the induction period, while the active sites cover the later stages of the induction period. Propylene is generated over the ZSM-5 (25) and ZSM-5 (36) catalysts. Correspondingly, there are low-temperature (LT), medium-temperature (MT), and high-temperature (HT) binding sites and low-temperature (LT), medium-temperature (MT), and high-temperature (HT) active sites. The binding sites are the first three site ensembles, and the active sites are the last three site ensembles. Over ZSM-5 (135) catalysts, there is no propylene formation, although six site ensembles exist.

Up to 3% of the overall acid sites are involved in the temperature-programmed surface reaction of methanol to primary olefins over fresh and working ZSM-5 catalysts. The binding sites, which account for 70% of these sites, are dominant. Conversely, up to 1% of the overall acid sites are involved in the temperature-programmed surface reaction of dimethyl ether over fresh and working ZSM-5 catalysts. The binding sites account for 30% of these sites (Tables 3 and 4), while the active sites, which account for 70% are dominant. During the induction period of propylene formation, the binding sites are relatively dominant with methanol, while the active sites are relatively dominant with dimethyl ether.

The crystallite size increases with an increase in the Si/Al ratio. ZSM-5 (135) catalysts have a higher crystallite size (0.78 ± 0.07 μm) compared to ZSM-5 (36), which has a crystallite size of (0.33 ± 0.05 μm), and ZSM-5 (25) catalysts, which have a crystallite size of (0.10 ± 0.02 μm). The acid site density decreases with an increase in the Si/Al ratio. ZSM-5 (135) catalysts have a BAS density of 78 μmol g⁻¹, while ZSM-5 (36) and ZSM-5 (25) have BAS densities of 117 and 428 μmol g⁻¹, respectively. The BET surface area reduces with an increase in the Si/Al ratio. ZSM-5 (135) catalysts have an apparent BET surface area of 358 m² g⁻¹, while ZSM-5 (36) catalysts have an apparent BET surface area of 410 m² g⁻¹ and ZSM-5 (25) catalysts have an apparent BET surface area of 413 m² g⁻¹.

Site-Specific Scaling Relations during the Induction Period. Many parameters have been extracted from the comparison of temperature-programmed surface reaction profiles and microkinetic model (see Sections S8–S13 of the Supporting Information) using the MTOTAPCAT code. We explore scaling relations between binding energies and reaction energies as well as between acid site density and binding energies or reaction energies. Site-specific scaling relations occur during

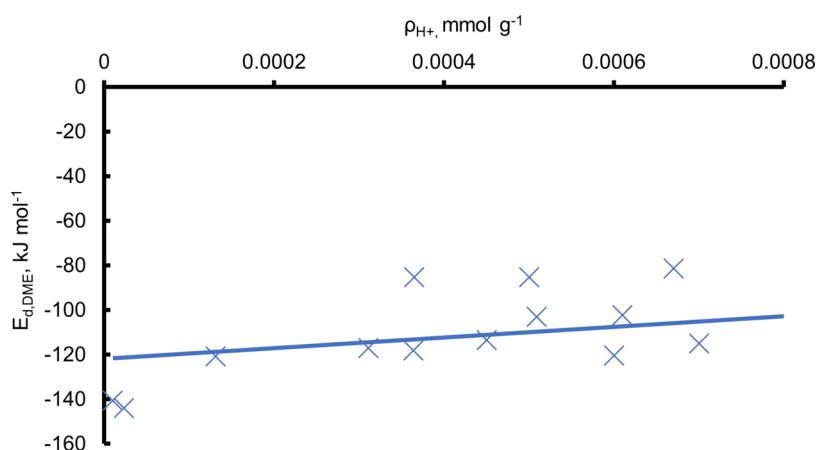


Figure 10. Scaling relations between the acid site density and the molecular adsorption of dimethyl ether over the low-temperature, medium-temperature, and high-temperature binding sites over fresh and working ZSM-5 (25), ZSM-5 (36), and ZSM-5 (135) catalysts during the temperature-programmed surface reaction of methanol.

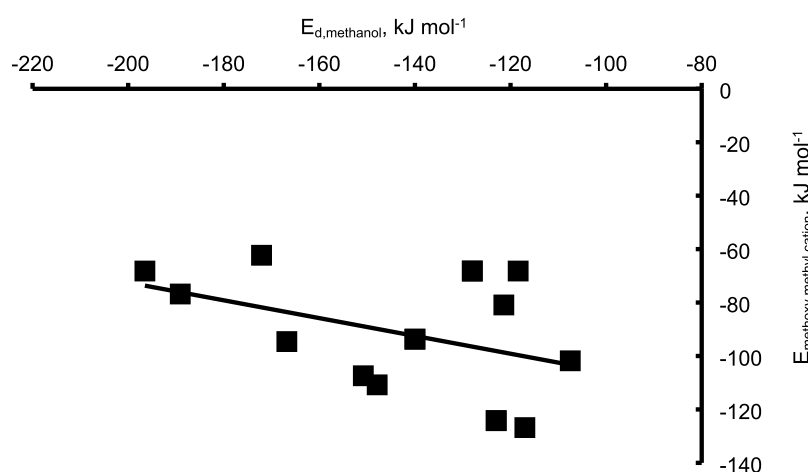


Figure 11. Scaling relations between the barriers of molecular adsorption of methanol and the formation of methoxy methyl cation over the low-temperature, medium-temperature, and high-temperature active sites over fresh and working ZSM-5 (25), ZSM-5 (36), and ZSM-5 (135) catalysts during the temperature-programmed surface reaction of methanol.

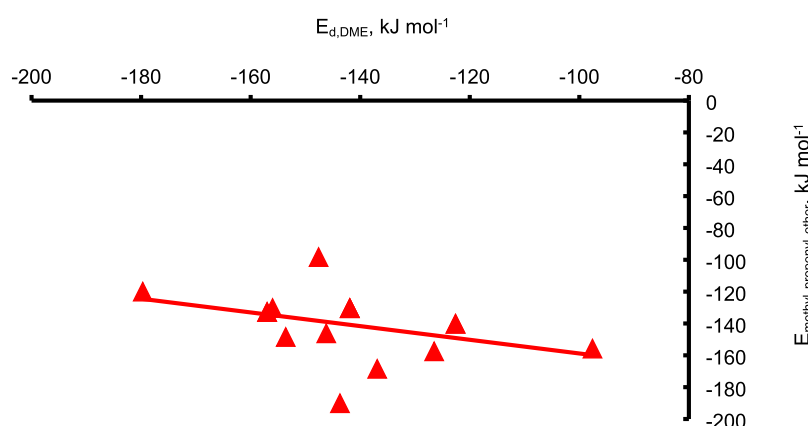


Figure 12. Scaling relations between the barriers of dissociative adsorption of dimethyl ether and the formation of methyl propenyl ether over the low-temperature, medium-temperature, and high-temperature active sites over fresh and working ZSM-5 (25), ZSM-5 (36), and ZSM-5 (135) catalysts during the temperature-programmed surface reaction of methanol.

the induction period of methanol and dimethyl ether over the binding sites and active sites of ZSM-5 catalysts.

Temperature-Programmed Surface Reaction of Methanol over ZSM-5 Catalysts. On the low-temperature, medium-temperature, and high-temperature binding sites of methanol

over fresh and working ZSM-5 catalysts, we observe scaling relations between the binding energy of dimethyl ether and the acid site density (Figure 10). Here, the binding energy of dimethyl ether is extracted from the molecular desorption of

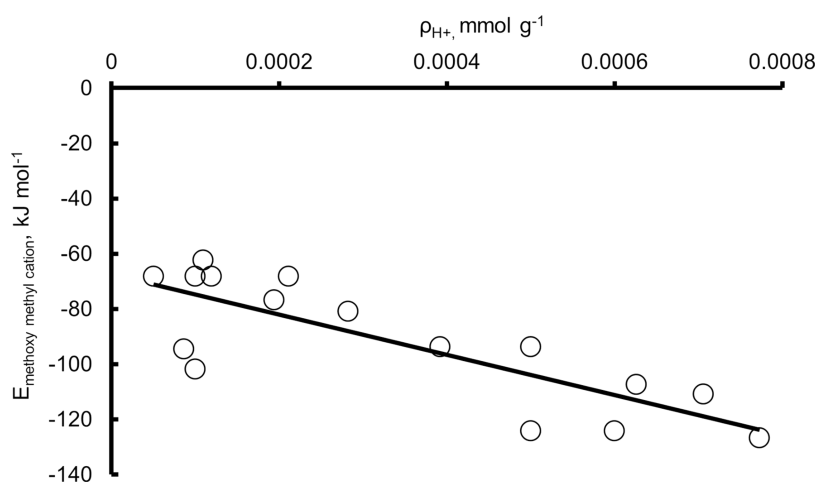


Figure 13. Scaling relations between the acid site density and barriers to the formation of methoxy methyl cation on the low-temperature, medium-temperature, and high-temperature active sites over fresh and working ZSM-5 (25), ZSM-5 (36), and ZSM-5 (135) catalysts during the temperature-programmed surface reaction of methanol.

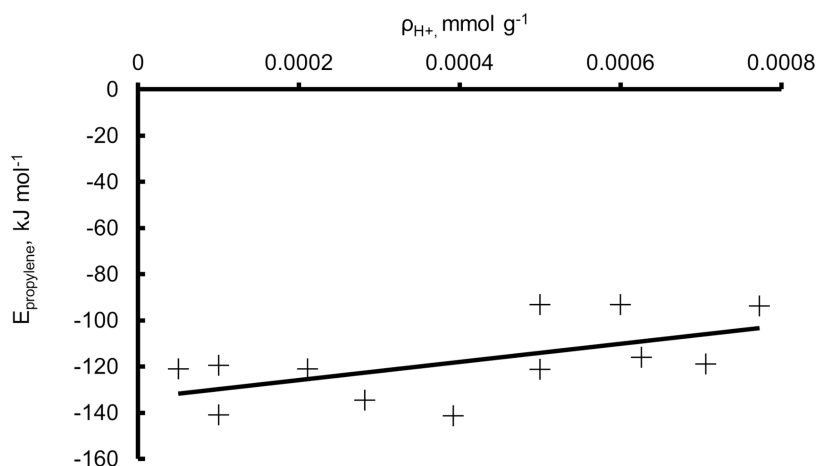


Figure 14. Scaling relations between the acid site density and barriers to the formation of propylene over low-temperature, medium-temperature, and high-temperature sites of ZSM-5 (25) and ZSM-5 (36) catalysts during the temperature-programmed surface reaction of methanol.

dimethyl ether on the different binding sites of the ZSM-5 catalyst.

In addition, we observe scaling relations between the binding energy of methanol and the barriers to the formation of methoxy methyl cation over the low-temperature, medium-temperature, and high-temperature active sites of ZSM-5 catalysts (Figure 11). The binding energy is extracted from the molecular desorption of methanol. Also, scaling relations are observed between the binding energy of dimethyl ether and the barriers to the formation of methyl propenyl ether (Figure 12). Here, the binding energy is extracted from the dissociative desorption of dimethyl ether.

We observe scaling relations between the acid site density and barriers to the formation of methoxy methyl cation and propylene over the low-temperature, medium-temperature, and high-temperature active sites during the induction period of methanol over ZSM-5 catalysts (Figures 13 and 14).

Over the binding sites, higher acid site densities are associated with lower barriers to dimethyl ether desorption (Figure 10) during the induction period of methanol conversion. Over the active sites, lower barriers to the molecular desorption of methanol correlate with higher barriers of methoxy methyl cation formation (Figure 11). In addition, lower barriers to the

dissociative desorption of dimethyl ether correlate with higher barriers of methyl propenyl ether formation (Figure 12). Furthermore, a higher site density (and thus shorter distance between acid sites) is associated with higher barriers to the formation of the methoxy methyl cation (Figure 13). Conversely, higher site densities are associated with lower barriers to propylene formation (Figure 14).

In summary, we show that during the induction period of methanol conversion over ZSM-5 catalysts, higher methanol and dimethyl ether binding energies and lower acid site densities are associated with lower barriers to methoxy methyl cation and methyl propenyl ether formation. Conversely, higher site densities correlate with lower barriers for propylene formation. Acid site density has the key influence on the reaction energies (Figures 13 and 14) and hence is the key descriptor over the active sites. Conversely, over the binding sites, a lower acid site density is associated with higher dimethyl ether binding energies. Acid site density is the key descriptor of the binding sites during the induction period of methanol conversion over ZSM-5 catalysts.

Temperature-Programmed Surface Reaction of Dimethyl Ether over ZSM-5 Catalysts. Over the low-, medium-, and high-temperature binding sites, we observe site-specific scaling

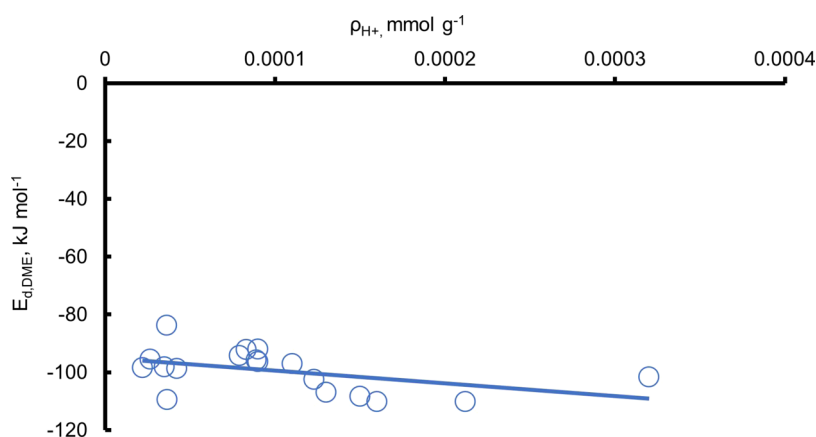


Figure 15. Scaling relations between the acid site density and the dissociative adsorption of dimethyl ether over the low-temperature, medium-temperature, and high-temperature binding sites over fresh and working ZSM-5 (25), ZSM-5 (36), and ZSM-5 (135) catalysts during the temperature-programmed surface reaction of dimethyl ether.

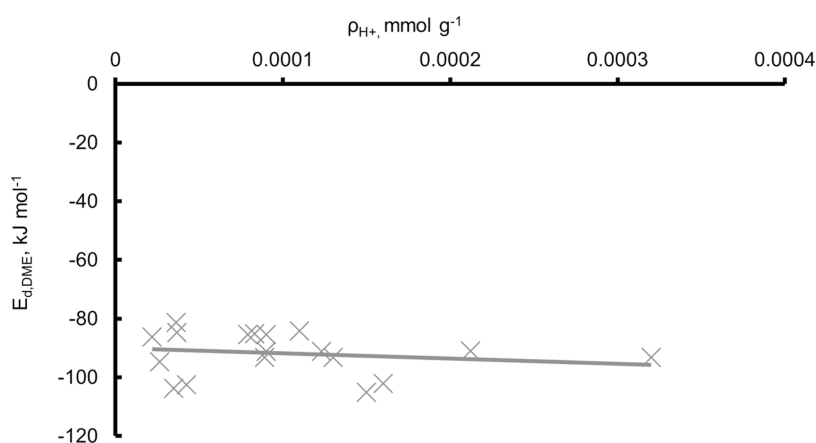


Figure 16. Scaling relations between the acid site density and the molecular adsorption of dimethyl ether over the low-temperature, medium-temperature, and high-temperature binding sites over fresh and working ZSM-5 (25), ZSM-5 (36), and ZSM-5 (135) catalysts during the temperature-programmed surface reaction of dimethyl ether.

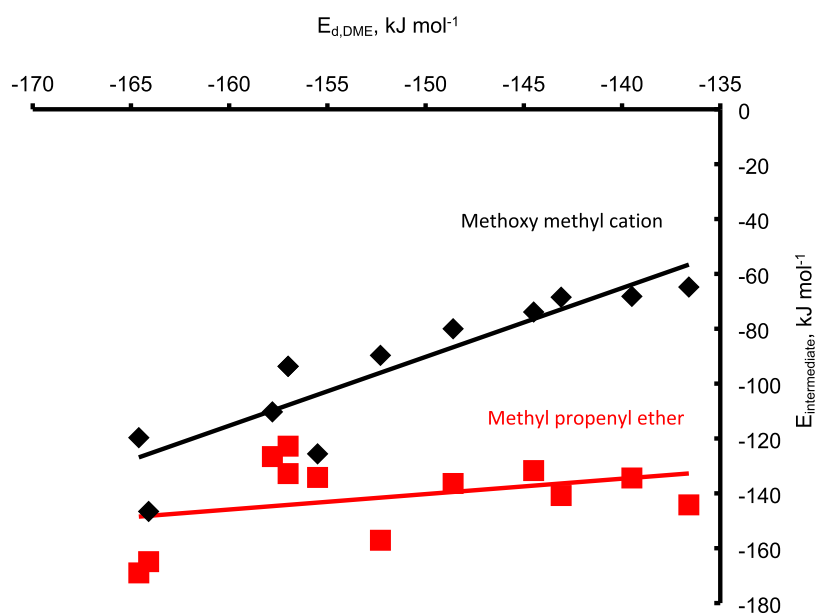


Figure 17. Scaling relations between the formation barriers of reaction intermediates of propylene formation as a function of activation energies of desorption of dimethyl ether over medium- and high-temperature active sites present on fresh and working ZSM-5 (25), ZSM-5 (36), and ZSM-5 (135) catalysts during the temperature-programmed surface reaction of dimethyl ether.

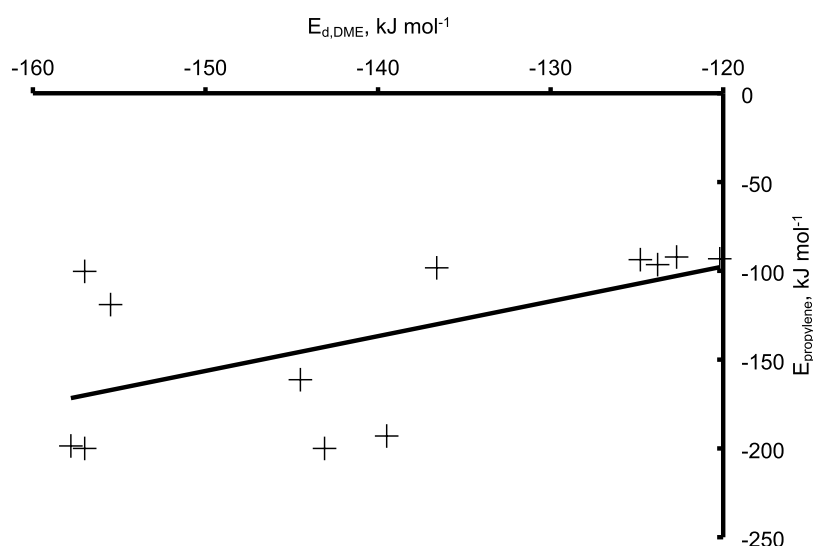


Figure 18. Scaling relations between the barriers of formation of propylene and activation energy of desorption of dimethyl ether over low-temperature, medium-temperature, and high-temperature active sites of fresh and working ZSM-5 (25) and ZSM-5 (36) catalysts during the temperature-programmed surface reaction of dimethyl ether.

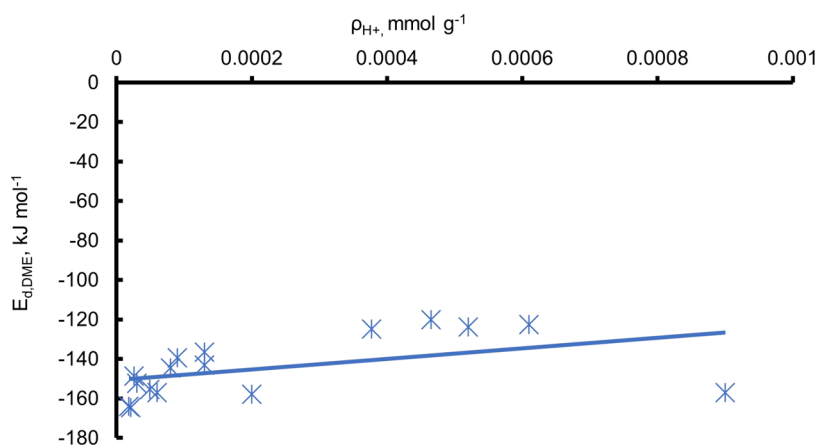


Figure 19. Scaling relations between the acid site density as a function of the activation energies of desorption of dimethyl ether over low-, medium-, and high-temperature active sites over fresh and working ZSM-5 (25), ZSM-5 (36), and ZSM-5 (135) catalysts during the temperature-programmed surface reaction of dimethyl ether.

relations between the binding energy of dimethyl ether to the ZSM-5 catalyst and the density of each site ensemble (Figure 15). Here, the binding energy of dimethyl ether is extracted from the dissociative adsorption of dimethyl ether. In addition, we observe similar scaling relations between the molecular adsorption of dimethyl ether and the acid site density (Figure 16).

We observe scaling relations between the binding energy of dimethyl ether to the ZSM-5 catalyst surface and the reaction energy of intermediates (methyl propenyl ether and methoxy methyl cation) leading up to the formation of propylene during the temperature-programmed surface reaction of dimethyl ether over fresh and working ZSM-5 catalysts. The binding energies of dimethyl ether are extracted from the dissociative adsorption of dimethyl ether on the different sites. These scaling relations are site-specific as they occur over the medium- and high-temperature active sites of ZSM-5 catalysts (Figure 17).

We observe scaling relations between the activation energy of desorption of dimethyl ether and the barriers to propylene formation over ZSM-5 catalysts (Figure 18). Here, the

activation energy of desorption is extracted from the dissociative adsorption of dimethyl ether on ZSM-5 catalysts.

We observe scaling relations between the density of acid sites and the binding energies of dimethyl ether to the surface of the ZSM-5 catalyst during the temperature-programmed surface reaction of dimethyl ether (Figure 19) over the low-temperature, medium-temperature, and high-temperature binding sites. Here, the binding energies of dimethyl ether are extracted from the dissociative adsorption of dimethyl ether on the different sites. The distance between acid sites is inversely proportional to the density of acid sites, i.e., $d_{\text{ave},\text{H}^+-\text{H}^+} \propto \rho_{\text{H}^+}^{-0.5}$ (eq 8). As the density of acid sites increases, the distance between acid sites decreases. We observe that a stronger binding energy of dimethyl ether with the acid sites correlates with a lower acid site density and a larger distance between acid sites.

Scaling relations are observed between the acid site density and the barriers to the formation of methyl propenyl ether during the induction period of dimethyl ether over ZSM-5 catalysts (Figure 20).

Over the binding sites, lower binding energies of dimethyl ether are observed at smaller site densities (Figures 15 and 16).

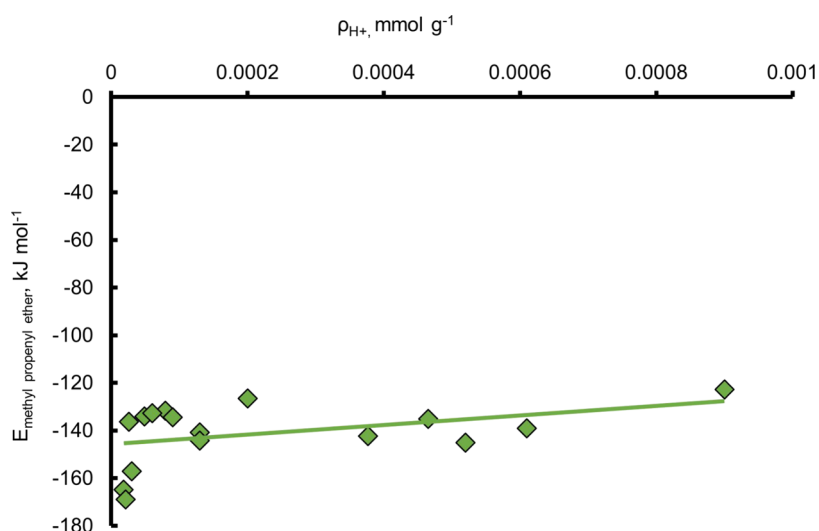


Figure 20. Scaling relations between the acid site density as a function of the barriers of the formation of methyl propenyl ether over low-, medium-, and high-temperature active sites for fresh and working ZSM-5 (25), ZSM-5 (36), and ZSM-5 (135) catalysts during the temperature-programmed surface reaction of dimethyl ether.

Over the active sites, lower binding energies of dimethyl ether lead to lower barriers to the formation of intermediates such as methoxy methyl cation and methyl propenyl ether (Figure 17). Higher activation energy of DME desorption is associated with lower barriers of propylene formation (Figure 18). Conversely, at the active sites, higher acid site densities are associated with lower barriers of DME desorption (Figure 19) and lower barriers to the formation of intermediates, methyl propenyl ether (Figure 20).

In summary, we show that during the induction period of dimethyl ether conversion over ZSM-5 catalysts, lower dimethyl ether binding energies and higher acid site densities are associated with lower reaction energies. The binding energy of dimethyl ether has the key influence on reaction intermediates and, hence, is the key descriptor (Figures 17 and 18). Lower binding energies of dimethyl ether are obtained at lower barriers of propylene formation. Conversely, on the binding sites, lower acid site densities are associated with lower binding energies of dimethyl ether.

The distance between acid sites is generally higher for fresh catalysts during the temperature-programmed surface reaction of dimethyl ether than for methanol. During the temperature-programmed surface reaction of dimethyl ether, they generally range from ca. 30 nm for high-temperature active sites over ZSM-5 (25) catalysts to ca. 120 nm for high-temperature active sites over ZSM-5 (36) catalysts and ca. 190 nm for high-temperature active sites over ZSM-5 (135) catalysts. During the temperature-programmed surface reaction of methanol, the distance between active sites ranges from ca. 37 nm for high-temperature active sites over ZSM-5 (25) catalysts to ca. 47 nm for high-temperature active sites over ZSM-5 (36) catalysts and ca. 83 nm for high-temperature active sites over ZSM-5 (135) catalysts.

In ZSM-5 catalysts, active site dynamics can be further incorporated through the elucidation of the clustering effects of water,^{60,61} or methanol,^{11,32} or proton hopping⁹ or the formation of organic reaction centers²⁹ and supramolecular structures.⁶² The nature and mobility of active sites affect the quantity of active sites. There are higher site densities and shorter acid site distances during the induction period of the

conversion of methanol compared to that of dimethyl ether over ZSM-5 catalysts. In our previous work,³² we observed that the adsorption stoichiometry is higher during the temperature-programmed desorption of methanol compared to that of dimethyl ether. This is attributed to the cluster formation of methanol molecules when adsorbing on ZSM-5 catalysts.¹¹ The shorter distances between acid sites show that the clusters on each site could form bonds. However, for dimethyl ether, a lower site density observed with longer distances between active sites gives fewer opportunities for cluster formation.

We observed that lower barriers of propylene formation are obtained at higher site densities during the induction period of methanol conversion. Evidently, the shorter distances between sites during the temperature-programmed surface reaction of methanol allow propagation of the formation of the primary olefin over ZSM-5 catalysts. The best correlation ($R^2 = 0.66$) exists between the acid site density and the barrier to the formation of methoxy methyl cation (Figure 13) during the induction period of methanol conversion over the low-temperature, medium-temperature, and high-temperature active sites of fresh and working ZSM-5 (25), ZSM-5 (36), and ZSM-5 (135) catalysts. During the induction period of dimethyl ether conversion over medium-temperature and high-temperature active sites of fresh and working ZSM-5 (25), (36), and ZSM-5 (135) catalysts, the best correlation ($R^2 = 0.79$) exists between the activation energy of DME desorption and the barrier to the formation of methoxy methyl cation (Figure 17). Consequently, acid site density and activation energies of DME desorption are key descriptors over the active sites during the induction period of propylene formation from methanol and dimethyl ether, respectively.

Over the binding sites on the low-temperature, medium-temperature, and high-temperature binding sites of fresh and working ZSM-5 (25), ZSM-5 (36), and ZSM-5 (135), the best correlation ($R^2 = 0.21$) occurs between the acid site density and dissociative desorption of dimethyl ether (Figure 15) during the induction period of dimethyl ether conversion. Over the binding sites on the low-, medium-, and high-temperature binding sites of fresh and working ZSM-5 (25), ZSM-5 (36), and ZSM-5 (135), the best correlation ($R^2 = 0.45$) occurs between the acid

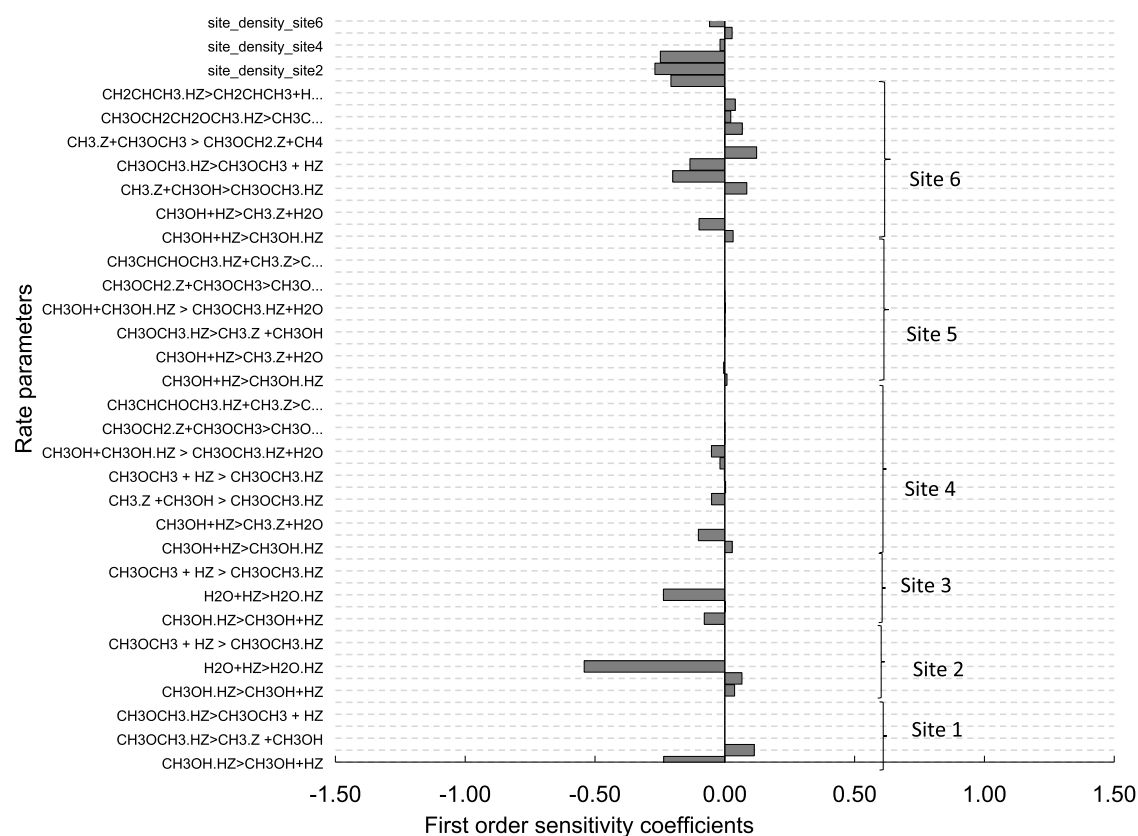


Figure 21. Sensitivity coefficient of rate parameters obtained for methanol TPSR over fresh ZSM-5 (36) catalysts.

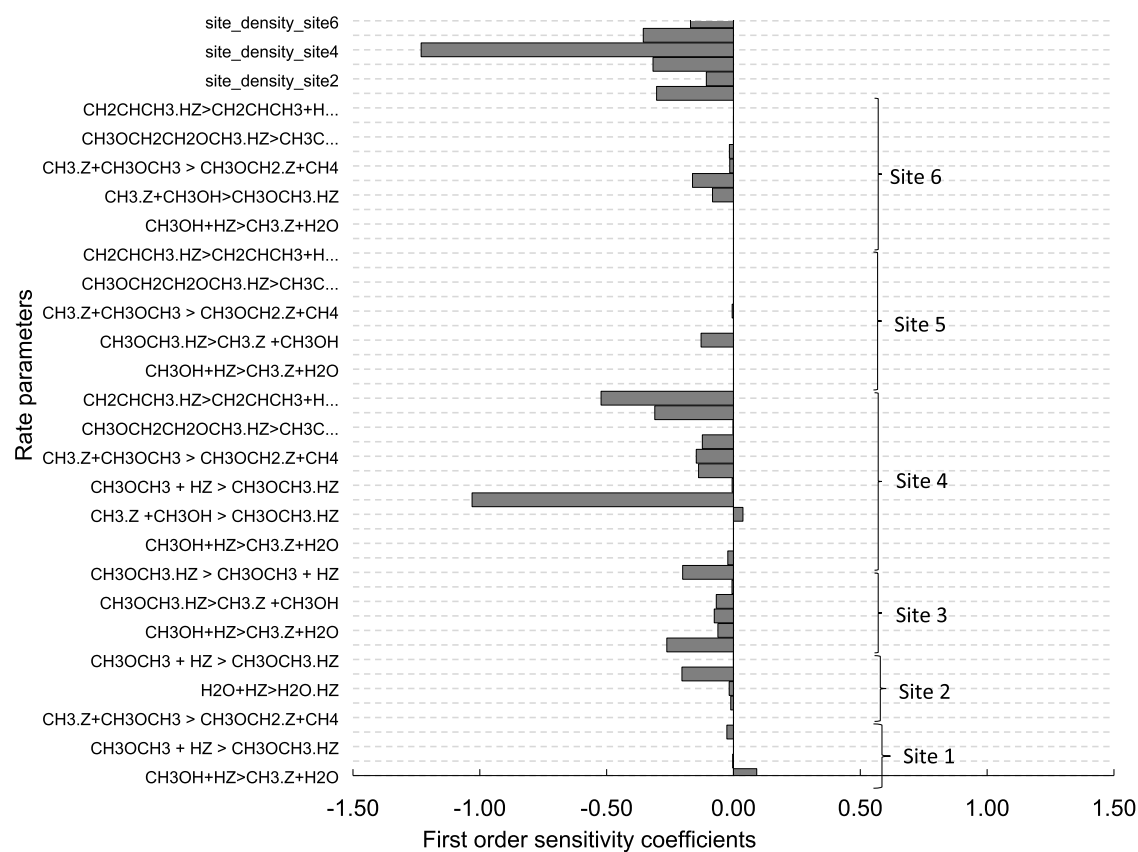


Figure 22. Sensitivity coefficient of rate parameters obtained for DME TPSR over fresh ZSM-5 (36) catalysts. Reproduced with permission from ref 41. Copyright 2021 Elsevier.

site density and the molecular desorption of methanol (Figure 10) during the induction period of methanol conversion. Consequently, acid site density is the key descriptor over the binding sites during the induction period of propylene formation from methanol and dimethyl ether.

Next, we examine the sensitivity of chemical steps during the temperature-programmed surface reaction of methanol and dimethyl ether over ZSM-5 catalysts.

■ SENSITIVITY ANALYSIS

Site 1 is the low-temperature binding site, site 2 is the medium-temperature binding site, and site 3 is the high-temperature binding site. Site 4 is the low-temperature active site, site 5 is the medium-temperature active site, and site 6 is the high-temperature active site. The sensitivity analysis shows that the low-, medium-, and high-temperature binding sites, which are activated between 300 and 450 K, are dominant during the induction period occurring during the temperature-programmed surface reaction of methanol (Figure 21). Water regulation through its adsorption on the medium- and high-temperature binding sites has the highest influence of all chemistries occurring in this temperature range. The chemistries involved in the high-temperature active site are influential in the formation of propylene during the temperature-programmed surface reaction of methanol.

During the temperature-programmed surface reaction of dimethyl ether, the low-temperature active sites (activated between 450 and 600 K) are dominant during the induction period (Figure 22). The dissociative desorption of dimethyl ether and the formation of adsorbed propylene as well as its molecular desorption on the low-temperature active site are the dominant chemistries during the temperature-programmed surface reaction of dimethyl ether over fresh and working catalysts.

Methanol behaves differently from dimethyl ether during the induction period of propylene formation over ZSM-5 catalysts. More water is formed during the induction period of methanol conversion compared with that of dimethyl ether. In general, higher site densities and shorter distances between acid sites are obtained for methanol compared with those of dimethyl ether. The binding sites are dominant during the induction period of the methanol conversion. Over these binding sites, lower acid site densities are associated with higher binding energies. Conversely, over the active sites, higher binding energies and lower acid site densities are associated with lower barriers to methoxy methyl cation and methyl propenyl ether formation during the induction period of methanol conversion over ZSM-5 catalysts. Higher site densities correlate with lower barriers to propylene formation. The dominant site ensemble during the induction period from methanol is the low-, medium-, and high-temperature binding sites (activated between 300 and 450 K) with water regulation through adsorption as the dominant chemistry on these sites. Acid site density is the key descriptor over both the binding sites and active sites of ZSM-5 catalysts during the induction period of methanol conversion.

The dominant site ensemble during the induction period of dimethyl ether is the low-temperature active site ensemble (activated between 450 and 600 K) with the dissociative desorption of dimethyl ether, the formation of adsorbed propylene, and molecular desorption as dominant chemistries over this site ensemble. The active sites are dominant during the induction period of dimethyl ether conversion. On these active sites, lower binding energies and higher acid site densities are

associated with lower reaction energies of methoxy methyl cation and methyl propenyl ether. Lower binding energies are obtained at lower barriers to propylene formation. Conversely, over the binding sites, lower acid site densities are associated with lower binding energies of dimethyl ether. While the acid site density is the key descriptor over the binding sites of ZSM-5 catalysts, the activation energy of desorption of dimethyl ether is the key descriptor over the active sites of the ZSM-5 catalyst during the induction period of dimethyl ether conversion.

Through microkinetic models, Nørskov and co-workers⁶³ observed scaling relations between adsorption energies and reaction energies, thus aiding the computational screening of catalysts. We observed site-specific scaling relations between the barriers of oxygenate desorption and reaction energies. These site-specific scaling relations can be used to optimize the size heterogeneity and distributions observed during the conversion of dimethyl ether to olefins over ZSM-5 catalysts. Murzin showed acid site density to be a descriptor over zeolites.⁵⁵ We showed above that acid site density is a descriptor during the induction period of methanol and dimethyl ether conversion over ZSM-5 catalysts. We observe site-specific scaling relations between acid site density and reaction energies during the induction period of propylene formation from methanol over ZSM-5 catalysts.

■ CONCLUSIONS

The induction period of the conversion of methanol and dimethyl ether to primary olefins over fresh and working ZSM-5 catalysts of different compositions, i.e., Si/Al ratios, has been studied using a combination of temperature-programmed surface reaction experiments and microkinetic modeling studies. Six ensembles of sites are observed: three binding site ensembles and three active site ensembles. During the temperature-programmed surface reaction of methanol over fresh and working ZSM-5 catalysts, these site ensembles account for up to 3% of the total sites present on the catalyst. Of these, ca. 70% are composed of the binding sites and ca. 30% are composed of active sites. The dominant site ensembles during the induction period of methanol conversion to propylene are the low-temperature, medium-temperature, and high-temperature binding sites activated between 300 and 450 K. However, during the temperature-programmed surface reaction of dimethyl ether over fresh and working ZSM-5 catalysts, the site ensembles account for up to 1% of the total sites on the catalyst. Binding sites account for ca. 30%, while active sites account for ca. 70% of these sites. The low-temperature active site activated between 450 and 600 K is the dominant site ensemble during the induction period of dimethyl ether conversion to olefins.

Acid site density and desorption barriers are key descriptors during the induction period of primary olefin formation over ZSM-5 catalysts. During the induction period of methanol conversion, the binding sites are more dominant. Over these binding sites, lower acid site densities are associated with higher activation energies of dimethyl ether desorption. Over the active sites, higher activation energies of methanol and dimethyl ether desorption are associated with lower barriers to methoxy methyl cation and methyl propenyl ether formation, respectively. Lower acid site densities correlate with lower barriers to methoxy methyl cation formation. Higher acid site densities correlate with lower barriers to propylene formation. During the induction period of dimethyl ether conversion, the active sites are the dominant site ensembles. Over these active sites, lower activation energies of dimethyl ether desorption and higher acid

site densities are associated with lower reaction energies of intermediate formation (methoxy methyl cation and methyl propenyl ether). Lower activation energies of DME desorption correlate with lower barriers to propylene formation. Over the binding sites, lower acid site densities correlate with lower activation energies for DME desorption. While the acid site density is the key descriptor during the induction period of methanol conversion, the barrier to dissociative desorption of dimethyl ether is the key descriptor during the induction period of dimethyl ether conversion over ZSM-5 catalysts. Barriers to propylene formation are lower during the induction period of methanol conversion (up to 141 kJ mol⁻¹) compared to that of dimethyl ether conversion (up to 200 kJ mol⁻¹). Site properties, via the acid site density, can be used to tune the induction period of the formation of propylene from methanol over ZSM-5 catalysts. Surface characteristics, through the activation energy of DME desorption, can be used to modulate the formation of propylene from dimethyl ether over ZSM-5 catalysts.

■ ASSOCIATED CONTENT

SI Supporting Information

The Supporting Information is available free of charge at <https://pubs.acs.org/doi/10.1021/acs.iecr.3c01401>

Sample TPSR profile, quantification of effluent, full TPSR profiles over ZSM-5 catalysts, a comparison of the TPSR of methanol to dimethyl ether, a comparison of fresh to working ZSM-5 catalysts during the TPSR of methanol and dimethyl ether, the effect of Si/Al ratios during the TPSR of methanol and dimethyl ether, a comparison of experiment to model during the temperature-programmed surface reaction of methanol and dimethyl ether over ZSM-5 catalysts of different Si/Al ratios, Tables S1–S36: kinetic parameters of the TPSR of methanol and DME over ZSM-5 of different compositions (PDF)

■ AUTHOR INFORMATION

Corresponding Author

Toyin Omojola – Department of Chemical Engineering, University of Bath, Bath BA2 7AY, U.K.; Present Address: Division of Fluid Dynamics, Department of Mechanics and Maritime Sciences, Chalmers University of Technology, SE 412–96 Gothenburg, Sweden; orcid.org/0000-0001-9376-6977; Email: toyin.omojola@bath.edu

Complete contact information is available at: <https://pubs.acs.org/doi/10.1021/acs.iecr.3c01401>

Notes

The author declares no competing financial interest.

■ ACKNOWLEDGMENTS

Funding from the Petroleum Technology Development Fund (PTDF/ED/PHD/OO/766/15) is acknowledged.

■ REFERENCES

- (1) Chang, C. D.; Silvestri, A. J. The conversion of methanol and other O-compounds to hydrocarbons over zeolite catalysts. *J. Catal.* **1977**, *47* (2), 249–259.
- (2) Koempel, H.; Liebner, W. Lurgi's Methanol To Propylene (MTP) Report on a successful commercialisation, in. *Stud. Surf. Sci. Catal.* **2007**, *167*, 261–267.
- (3) Haag, S.; Pohl, S.; Gorny, M.; Rothaemel, M. Methanol to Propylene: From Development to Commercialization. in DGMK Conference: Reducing the Carbon Footprint of Fuels and Petrochemicals, Berlin, Germany. 2012.
- (4) Chang, C. D.; Lang, W. H.; Smith, R. L. The conversion of methanol and other O-compounds to hydrocarbons over zeolite catalysts. II. Pressure effects. *J. Catal.* **1979**, *56* (2), 169–173.
- (5) Chu, C. T. W.; Chang, C. D. Methanol conversion to olefins over ZSM-5. II. Olefin distribution. *J. Catal.* **1984**, *86* (2), 297–300.
- (6) Omojola, T.; Lukyanov, D. B.; Cherkasov, N.; Zholobenko, V. L.; van Veen, A. C. Influence of Precursors on the Induction Period and Transition Regime of Dimethyl Ether Conversion to Hydrocarbons over ZSM-5 Catalysts. *Ind. Eng. Chem. Res.* **2019**, *58* (36), 16479–16488.
- (7) Svelle, S.; Joensen, F.; Nerlov, J.; Olsbye, U.; Lillerud, K. P.; Kolboe, S.; Bjørgen, M. Conversion of methanol into hydrocarbons over zeolite H-ZSM-5: Ethene formation is mechanistically separated from the formation of higher alkenes. *J. Am. Chem. Soc.* **2006**, *128* (46), 14770–14771.
- (8) Bjørgen, M.; Svelle, S.; Joensen, F.; Nerlov, J.; Kolboe, S.; Bonino, F.; Palumbo, L.; Bordiga, S.; Olsbye, U. Conversion of methanol to hydrocarbons over zeolite H-ZSM-5: On the origin of the olefinic species. *J. Catal.* **2007**, *249* (2), 195–207.
- (9) Ryder, J. A.; Chakraborty, A. K.; Bell, A. T. Density functional theory study of proton mobility in zeolites: Proton migration and hydrogen exchange in ZSM-5. *J. Phys. Chem. B* **2000**, *104* (30), 6998–7011.
- (10) Nastase, S. A. F.; Cnudde, P.; Vanduyfhuys, L.; De Wispelaere, K.; Van Speybroeck, V.; Catlow, C. R. A.; Logsdail, A. J. Mechanistic insight into the framework methylation of H-ZSM-5 for varying methanol loading and Si/Al ratio using first principles molecular dynamics simulations. *ACS Catal.* **2020**, *15*, 8904–8915, DOI: 10.1021/acscatal.0c01454.
- (11) Mirth, G.; Lercher, J. A.; Anderson, M. W.; Klinowski, J. Adsorption complexes of methanol on zeolite ZSM-5. *J. Chem. Soc., Faraday Trans.* **1990**, *86* (17), 3039–3044.
- (12) Yamazaki, H.; Shima, H.; Imai, H.; Yokoi, T.; Tatsumi, T.; Kondo, J. N. Evidence for a "carbene-like" intermediate during the reaction of methoxy species with light alkenes on H-ZSM-5. *Angew. Chem., Int. Ed.* **2011**, *50* (8), 1853–1856.
- (13) Sinclair, P. E.; Catlow, C. R. A. Generation of carbenes during methanol conversion over Bronsted acidic aluminosilicates. A computational study. *J. Phys. Chem. B* **1997**, *101* (3), 295–298.
- (14) Yamazaki, H.; Shima, H.; Imai, H.; Yokoi, T.; Tatsumi, T.; Kondo, J. N. Direct production of propene from methoxy species and dimethyl ether over H-ZSM-5. *J. Phys. Chem. C* **2012**, *116* (45), 24091–24097.
- (15) Lesthaeghe, D.; Van Speybroeck, V.; Marin, G. B.; Waroquier, M. What role do oxonium ions and oxonium ylides play in the ZSM-5 catalysed methanol-to-olefin process? *Chem. Phys. Lett.* **2006**, *417* (4–6), 309–315.
- (16) Hutchings, G. J.; Gottschalk, F.; Hunter, R. Comments on "kinetic model for methanol conversion to olefins" with respect to methane formation at low conversion. *Ind. Eng. Chem. Res.* **1987**, *26* (3), 635–637.
- (17) Hutchings, G. J.; Gottschalk, F.; Hall, M. V. M.; Hunter, R. Hydrocarbon formation from methylating agents over the zeolite catalyst ZSM-5. Comments on the mechanism of carbon-carbon bond and methane formation. *J. Chem. Soc., Faraday Trans. 1* **1987**, *83* (3), 571–583.
- (18) Wu, X.; Xu, S.; Zhang, W.; Huang, J.; Li, J.; Yu, B.; Wei, Y.; Liu, Z. Direct Mechanism of the First Carbon–Carbon Bond Formation in the Methanol-to-Hydrocarbons Process. *Angew. Chem., Int. Ed.* **2017**, *56* (31), 9039–9043.
- (19) Wang, W.; Buchholz, A.; Seiler, M.; Hunger, M. Evidence for an Initiation of the Methanol-to-Olefin Process by Reactive Surface Methoxy Groups on Acidic Zeolite Catalysts. *J. Am. Chem. Soc.* **2003**, *125* (49), 15260–15267.

- (20) Jiang, Y.; Wang, W.; Marthala, V. R. R.; Huang, J.; Sulikowski, B.; Hunger, M. Effect of organic impurities on the hydrocarbon formation via the decomposition of surface methoxy groups on acidic zeolite catalysts. *J. Catal.* **2006**, *238* (1), 21–27.
- (21) Jiang, Y.; Hunger, M.; Wang, W. On the reactivity of surface methoxy species in acidic zeolites. *J. Am. Chem. Soc.* **2006**, *128* (35), 11679–11692.
- (22) Li, J.; Wei, Z.; Chen, Y.; Jing, B.; He, Y.; Dong, M.; Jiao, H.; Li, X.; Qin, Z.; Wang, J.; Fan, W. A route to form initial hydrocarbon pool species in methanol conversion to olefins over zeolites. *J. Catal.* **2014**, *317* (0), 277–283.
- (23) Wei, Z.; Chen, Y. Y.; Li, J.; Guo, W.; Wang, S.; Dong, M.; Qin, Z.; Wang, J.; Jiao, H.; Fan, W. Stability and Reactivity of Intermediates of Methanol Related Reactions and C–C Bond Formation over H-ZSM-5 Acidic Catalyst: A Computational Analysis. *J. Phys. Chem. C* **2016**, *120* (11), 6075–6087.
- (24) Chowdhury, A. D.; Houben, K.; Whiting, G. T.; Mokhtar, M.; Asiri, A. M.; Al-Thabaiti, S. A.; Basahel, S. N.; Baldus, M.; Weckhuysen, B. M. Initial Carbon–Carbon Bond Formation during the Early Stages of the Methanol-to-Olefin Process Proven by Zeolite-Trapped Acetate and Methyl Acetate. *Angew. Chem., Int. Ed.* **2016**, *55* (51), 15840–15845.
- (25) Chowdhury, A. D.; Paioni, A. L.; Houben, K.; Whiting, G. T.; Baldus, M.; Weckhuysen, B. M. Bridging the Gap between the Direct and Hydrocarbon Pool Mechanisms of the Methanol-to-Hydrocarbons Process. *Angew. Chem., Int. Ed.* **2018**, 8095–8099, DOI: 10.1002/anie.201803279.
- (26) Plessow, P. N.; Studt, F. Unraveling the Mechanism of the Initiation Reaction of the Methanol to Olefins Process Using ab Initio and DFT Calculations. *ACS. Catalysis* **2017**, *7* (11), 7987–7994.
- (27) Plessow, P. N.; Smith, A.; Tischer, S.; Studt, F. Identification of the Reaction Sequence of the MTO Initiation Mechanism Using Ab Initio-Based Kinetics. *J. Am. Chem. Soc.* **2019**, *141* (14), 5908–5915.
- (28) Liu, Y.; Müller, S.; Berger, D.; Jelic, J.; Reuter, K.; Tonigold, M.; Sanchez-Sanchez, M.; Lercher, J. A. Formation Mechanism of the First Carbon–Carbon Bond and the First Olefin in the Methanol Conversion into Hydrocarbons. *Angew. Chem., Int. Ed.* **2016**, *55* (19), 5723–5726.
- (29) Haw, J. F.; Song, W.; Marcus, D. M.; Nicholas, J. B. The Mechanism of Methanol to Hydrocarbon Catalysis. *Acc. Chem. Res.* **2003**, *36*, 317–326.
- (30) Wang, C.; Wang, Q.; Xu, J.; Qi, G.; Gao, P.; Wang, W.; Zou, Y.; Feng, N.; Liu, X.; Deng, F. Direct Detection of Supramolecular Reaction Centers in the Methanol-to-Olefins Conversion over Zeolite H-ZSM-5 by ¹³C-27Al Solid-State NMR Spectroscopy. *Angew. Chem., Int. Ed.* **2016**, *55* (7), 2507–2511.
- (31) Grifoni, E.; Piccini, G.; Lercher, J. A.; Glezakou, V. A.; Rousseau, R.; Parrinello, M. Confinement effects and acid strength in zeolites. *Nat. Commun.* **2021**, *12* (1), No. 2630.
- (32) Omojola, T.; Cherkasov, N.; McNab, A. I.; Lukyanov, D. B.; Anderson, J. A.; Rebrov, E. V.; van Veen, A. C. Mechanistic Insights into the Desorption of Methanol and Dimethyl Ether Over ZSM-5 Catalysts. *Catal. Lett.* **2018**, *148* (1), 474–488.
- (33) Hack, J. H.; Dombrowski, J. P.; Ma, X.; Chen, Y.; Lewis, N. H. C.; Carpenter, W. B.; Li, C.; Voth, G. A.; Kung, H. H.; Tokmakoff, A. Structural Characterization of Protonated Water Clusters Confined in HZSM-5 Zeolites. *J. Am. Chem. Soc.* **2021**, *143* (27), 10203–10213.
- (34) Bocus, M.; Neale, S. E.; Cnudde, P.; Van, V. Speybroeck, Dynamic evolution of catalytic active sites within zeolite catalysis, in Reference Module in Chemistry. In *Molecular Sciences and Chemical Engineering*; Elsevier, 2021.
- (35) Li, C.; Ferri, P.; Paris, C.; Moliner, M.; Boronat, M.; Corma, A. Design and Synthesis of the Active Site Environment in Zeolite Catalysts for Selectively Manipulating Mechanistic Pathways. *J. Am. Chem. Soc.* **2021**, *143*, 10718–10726, DOI: 10.1021/jacs.1c04818.
- (36) Zhang, Q.; Yu, J.; Corma, A. Applications of Zeolites to C1 Chemistry: Recent Advances, Challenges, and Opportunities. *Adv. Mater.* **2020**, *32* (44), No. 2002927.
- (37) Dib, E.; Grand, J.; Gedeon, A.; Mintova, S.; Fernandez, C. Control the position of framework defects in zeolites by changing the symmetry of organic structure directing agents. *Microporous Mesoporous Mater.* **2021**, *315*, No. 110899.
- (38) Li, C.; Moliner, M.; Corma, A. Building Zeolites from Precrystallized Units: Nanoscale Architecture. *Angew. Chem., Int. Ed.* **2018**, *57* (47), 15330–15353.
- (39) Omojola, T.; van Veen, A. C. Competitive adsorption of oxygenates and aromatics during the initial steps of the formation of primary olefins over ZSM-5 catalysts. *Catal. Commun.* **2020**, *140*, No. 106010, DOI: 10.1016/j.catcom.2020.106010.
- (40) Omojola, T. Site-specific scaling relations observed during methanol-to-olefin conversion over ZSM-5 catalysts. *Chem. Eng. Sci.* **2022**, *251*, No. 117424, DOI: 10.1016/j.ces.2022.117424.
- (41) Omojola, T.; van Veen, A. C. Mechanistic insights into the conversion of dimethyl ether over ZSM-5 catalysts: A combined temperature-programmed surface reaction and microkinetic modelling study. *Chem. Eng. Sci.* **2021**, *239*, No. 116620.
- (42) Omojola, T.; Lukyanov, D. B.; van Veen, A. C. Transient kinetic studies and microkinetic modeling of primary olefin formation from dimethyl ether over ZSM-5 catalysts. *Int. J. Chem. Kinet.* **2019**, *51* (7), 528–537.
- (43) Omojola, T.; Silverwood, I. P.; O'Malley, A. J. Molecular behaviour of methanol and dimethyl ether in H-ZSM-5 catalysts as a function of Si/Al ratio: a quasielastic neutron scattering study. *Catal. Sci. Technol.* **2020**, *10* (13), 4305–4320.
- (44) Porter, A. J.; McHugh, S. L.; Omojola, T.; Silverwood, I. P.; O'Malley, A. J. The effect of Si/Al ratio on local and nanoscale water diffusion in H-ZSM-5: A quasielastic neutron scattering and molecular dynamics simulation study. *Microporous Mesoporous Mater.* **2023**, *348*, No. 112391.
- (45) Gleaves, J. T.; Ebner, J. R.; Kuechler, T. C. Temporal Analysis of Products (TAP) — A Unique Catalyst Evaluation System with Submillisecond Time Resolution. *Catal. Rev.* **1988**, *30* (1), 49–116.
- (46) Van Veen, A. C.; Zanthoff, H. W.; Hinrichsen, O.; Muhler, M. Fixed-bed microreactor for transient kinetic experiments with strongly adsorbing gases under high vacuum conditions. *J. Vac. Sci. Technol., A* **2001**, *19* (2), 651–655.
- (47) Marin, G. B.; Yablonsky, G. S., Kinetics of Chemical Reactions: Decoding Complexity. 2011, WILEY-VCH, Weinheim, Germany. 1–428.
- (48) Omojola, T. Experimental and Kinetic Modelling Studies of Methanol Conversion to Hydrocarbons over Zeolite Catalysts, in *Chemical Engineering*; University of Bath, 2019; p 363.
- (49) Omojola, T.; Logsdail, A. J.; van Veen, A. C.; Nastase, S. A. F. A quantitative multiscale perspective on primary olefin formation from methanol. *Phys. Chem. Chem. Phys.* **2021**, *23* (38), 21437–21469.
- (50) Courant, R.; Friedrichs, K.; Lewy, H. Über die partiellen Differenzgleichungen der mathematischen Physik. *Math. Ann.* **1928**, *100* (1), 32–74.
- (51) Van Der Linde, S. C.; Nijhuis, T. A.; Dekker, F. H. M.; Kapteijn, F.; Moulijn, J. A. Mathematical treatment of transient kinetic data: Combination of parameter estimation with solving the related partial differential equations. *Appl. Catal., A* **1997**, *151* (1), 27–57.
- (52) Rasmuson, A.; Andersson, B.; Olsson, L.; Andersson, R. *Mathematical Modeling in Chemical Engineering*; Cambridge University Press: USA, 2014.
- (53) Lagarias, J. C.; Reeds, J. A.; Wright, M. H.; Wright, P. E. Convergence properties of the Nelder-Mead simplex method in low dimensions. *SIAM J. Optimization* **1998**, *9* (1), 112–147.
- (54) Gayubo, A. G.; Alonso, A.; Valle, B.; Aguayo, A. T.; Bilbao, J. Kinetic Model for the Transformation of Bioethanol into Olefins over a HZSM-5 Zeolite Treated with Alkali. *Ind. Eng. Chem. Res.* **2010**, *49* (21), 10836–10844.
- (55) Murzin, D. Y. Acid Site Density as a Kinetic Descriptor of Catalytic Reactions over Zeolites. *Chemistry* **2022**, *4* (4), 1609–1623.
- (56) Murzin, D. Y. Kinetics of Heterogeneous Single-Site Catalysis. *ChemCatChem* **2023**, *15* (1), No. e202201082, DOI: 10.1002/cctc.202201082.
- (57) Matam, S. K.; Howe, R. F.; Thetford, A.; Catlow, C. R. A. Room temperature methoxylation in zeolite H-ZSM-5: an operando

DRIFTS/mass spectrometric study. *Chem. Commun.* **2018**, *54* (91), 12875–12878.

(58) O'Malley, A.; Parker, S. F.; Chutia, A.; Farrow, M. R.; Silverwood, I. P.; Garcia-Sakai, V.; Catlow, C. R. A. Room temperature methoxylation in zeolites: insight into a key step of the methanol-to-hydrocarbons process. *ChemComm* **2016**, *52*, 2897–2900.

(59) Song, W.; Marcus, D. M.; Fu, H.; Ehresmann, J. O.; Haw, J. F. An oft-studied reaction that may never have been: Direct catalytic conversion of methanol or dimethyl ether to hydrocarbons on the solid acids HZSM-5 or HSAPO-34. *J. Am. Chem. Soc.* **2002**, *124* (15), 3844–3845.

(60) Pfriem, N.; Hintermeier, P. H.; Eckstein, S.; Kim, S.; Liu, Q.; Shi, H.; Milakovic, L.; Liu, Y.; Haller, G. L.; Baráth, E.; Liu, Y.; Lercher, J. A. Role of the ionic environment in enhancing the activity of reacting molecules in zeolite pores. *Science* **2021**, *372* (6545), 952–957, DOI: 10.1126/science.abh3418.

(61) Eckstein, S.; Hintermeier, P. H.; Zhao, R.; Baráth, E.; Shi, H.; Liu, Y.; Lercher, J. A. Influence of Hydronium Ions in Zeolites on Sorption. *Angew. Chem., Int. Ed.* **2019**, *58* (11), 3450–3455.

(62) Lin, S.; Zhi, Y.; Chen, W.; Li, H.; Zhang, W.; Lou, C.; Wu, X.; Zeng, S.; Xu, S.; Xiao, J.; Zheng, A.; Wei, Y.; Liu, Z. Molecular Routes of Dynamic Autocatalysis for Methanol-to-Hydrocarbons Reaction. *J. Am. Chem. Soc.* **2021**, *143*, 12038–12052, DOI: 10.1021/jacs.1c03475.

(63) Ulissi, Z. W.; Medford, A. J.; Bligaard, T.; Nørskov, J. K. To address surface reaction network complexity using scaling relations machine learning and DFT calculations. *Nat. Commun.* **2017**, *8*, No. 14621.

Recommended by ACS

Diffusion and Reaction in Foam-Based Catalysts: Effectiveness Factor Expressions for LHHW, Nonisothermal and General Order Kinetics

Minaz Makhania and Sreedevi Upadhyayula

SEPTEMBER 29, 2023

INDUSTRIAL & ENGINEERING CHEMISTRY RESEARCH

READ 

ZSM-22 Synthesized Using Structure-Directing Agents of Different Alkyl Chain Lengths for Controlled *n*-Hexadecane Hydroisomerizations

Qiang Wang, Binghui Chen, *et al.*

JULY 12, 2023

INDUSTRIAL & ENGINEERING CHEMISTRY RESEARCH

READ 

Revealing Main Reaction Paths to Olefins and Aromatics in Methanol-to-Hydrocarbons over H-ZSM-5 by Isotope Labeling

Chuncheng Liu, Freek Kapteijn, *et al.*

MARCH 30, 2023

ACS CATALYSIS

READ 

Mathematical Model for the Industrial SMTO Reactor with a SAPO-34 Catalyst

Hongbo Jiang, Yushi Chen, *et al.*

MARCH 03, 2023

ACS OMEGA

READ 

Get More Suggestions >